5. SITE 1121: THE CAMPBELL "DRIFT"[1]
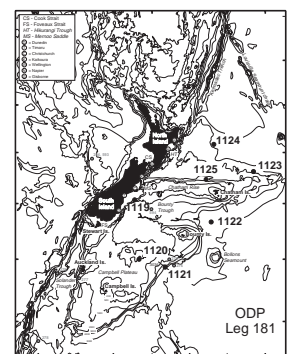
Shipboard Scientific Party[2]

BACKGROUND AND OBJECTIVES

The principal results for this site bear little relationship to the proposed objectives. If these objectives had read, "Determine whether the Campbell Drift is actually a Neogene contourite drift," we could at least have declared a limited success with the answer, "At least the top 10 to 30 m is strongly current influenced, but it represents 10 to 20 m.y." Henceforth, in this instance, Campbell "drift" will require quotation marks.

General Description

Carter and McCave (1997) introduced the name "Campbell Drift" for an extensive sediment accumulation up to 170 km wide, 850 km long, and a maximum of 1.1-s thickness, which occurs along the margin of the Campbell Plateau at depths of 4000–4800 m. It sits under the path of the combined Deep Western Boundary Current (DWBC) and Antarctic Circumpolar Current (ACC). Site 1121 lies downstream of the first significant input of sediment to the DWBC, namely from turbidity currents flowing down Solander Channel into Emerald Basin to the west of Campbell Plateau (Carter and McCave, 1997) (Fig. F1). Scour in the Emerald Basin provides sediment that was presumed to be transported over the Campbell "drift" and partly deposited there. Part of the powerful ACC detaches from the Campbell Plateau boundary at ~55°S (Orsi et al., 1995), but the rest of this flow continues north to Bollons Seamount, where it too veers east to eventually link with the southern branch. Further north, still more tranquil conditions occur under the DWBC alone. Under the ACC, the seabed shows signs of scour and slow deposition in an extensive field of ferromanganese nodules and pavement (Carter, 1989).

F1. Location of Site 1121 and seismic line NIWA 3034, p. 27.

The underlying crust at Site 1121 dates from the rifting of Campbell Plateau from Marie Byrd Land at 85 Ma (Lawver and Gahagan, 1994). Immediately overlying that crust is up to ~1000 m of sediment, presumed to be a wedge of nonmarine clastics followed by uppermost Cretaceous and Paleogene marine sediments and Neogene contourites. In particular, Carter and McCave (1997) surmised that the uppermost sequence of closely spaced reflectors (~160 m thick) was of Pliocene–Pleistocene age. DSDP Site 276 was located in the erosional moat between the western edge of the "drift" and the Campbell Plateau escarpment; sampled gravel, sand, and a few rock chips suggest the presence of underlying siliceous siltstones. DWBC/ACC erosion has apparently cut down to the Paleogene in the moat, apart from a thin skin of sediment smeared on the drill bit that bears Miocene to Pleistocene microfossils (Kennett, Houtz, et al., 1975). It was thought that this indicated a good chance of obtaining a continuous Neogene–Paleogene section by drilling through the crest of the "drift" at Site 1121. Such a section would record the history of the ACC-DWBC and associated water masses as they approached the Southwest Pacific gateway.

There are few modern seismic profiles across the area. Older *Eltanin* profiles reveal only one shallow reflector, thought to delimit Pliocene–Pleistocene strata. Modern multichannel data show two principal reflectors, which lie close to the levels drilled, the first at a seafloor depth of ~120 ms two-way traveltime (TWT), 90–100 m, and the second (R1) at 316 ms TWT or ~250 to 300 m, depending on velocity (Fig. F2). Before drilling, the deeper of these was inferred to represent mid- to late Oligocene erosion. The upper reflector is not truncated in the moat along the foot of the scarp and thus fails to indicate profound erosion.

Site Objectives

Site 1121 was drilled to obtain a sediment record of flow and sediment supply changes in the DWBC system. Special interest was to be focused on a comparison of paleocurrent speeds between this site and sites farther north, as Site 1121 is located where the DWBC is presently reinforced by the ACC. It was intended that this comparison would allow the effects of the ACC and DWBC to be distinguished. This site, uniquely among the sites planned to be drilled on Leg 181, was hoped to yield data pertaining to the deepest layer of the DWBC which originates mainly as Weddell Sea Deep Water.

OPERATIONS

Hole 1121A

The 95-nmi voyage to Site 1121 (proposed site SWPAC-7B) was accomplished at an average speed of 10.4 kt. The vessel proceeded directly to the Global Positioning System coordinates of the location. The positioning beacon was dropped at 2025 hr on 1 September. A backup beacon with a higher output setting had to be launched because the first beacon signal was marginal. The hydrophones and thrusters were lowered and the advanced hydraulic piston corer/extended core barrel (APC/XCB) bottom-hole assembly was assembled using a 9-⅞-in PDC bit and deployed. A drill pipe swab (pig) was pumped down the pipe to clean out rust that had accumulated in the additional drill pipe that was brought for this deep-water site. Hole 1121A was spudded with

F2. Part of seismic profile NIWA 3034, **p. 28.**
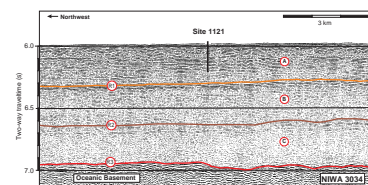
the APC at 1554 hr on 2 September. The recovery indicated that the water depth was 4492 m below sea level (mbsl). The hole was scheduled for only a mudline sample, and the single APC Core 1H was taken from 0 to 8.4 mbsf (Table T1, also in ASCII format).

Hole 1121B

The second hole of the site was spudded with the APC at 1710 hr on 2 September. The seafloor depth inferred from recovery was 4487.9 mbsl. APC coring advanced to 23.0 mbsf when Core 3H did not achieve a full stroke (Table T1). The XCB barrel was run in with a soft formation cutting shoe and experienced considerable difficulty advancing with high torque and a very low penetration rate. After advancing only 0.5 m in 30 min of rotation, the core barrel was recovered to investigate why the coring was so difficult. The core proved to contain chert fragments. A hard-formation cutting shoe was deployed, and coring continued with the XCB in slow and occasionally difficult conditions.

Coring by XCB had deepened the hole to 139.7 mbsf when operations were terminated because the scientific objectives were reached. The bit cleared the seafloor at 0120 hr on 4 September, ending operations at Hole 1121B. The bit was at the plane of the rotary table at 1040 hr and by 1045 hr the drilling equipment was secured for the voyage to the next site. Both beacons were recalled and recovered. At 1045 hr on 4 September, the vessel was under way on a northeasterly course to Site 1122.

LITHOSTRATIGRAPHY

Introduction

Site 1121 was planned to penetrate a sedimentary body deposited along the foot of the Campbell Plateau in water depths of 4400 to 4600 m. This deposit was initially delimited from a suite of single-channel air gun profiles run by the *Eltanin* in the 1960s and 1970s. One of these profiles, *Eltanin* line 43, was used to guide Site 276, drilled during DSDP Leg 29 (Kennett, Houtz, et al., 1975). This site was located at 4761 m depth within a scour moat eroded along the base of the plateau. There, the drill string penetrated a current-swept lag deposit of gravelly sand and recovered a few rock chips probably derived from underlying Paleogene siliceous siltstones (Kennett, Houtz, et al., 1975). A resume of the DSDP and *Eltanin* data sets by Carter and McCave (1997) concluded that the moat had been eroded by a fast-flowing core of the Deep Western Boundary Current (DWBC) in consort with the Antarctic Circumpolar Current (ACC). East of the moat, the seismic profiles were interpreted to show sediment deposited to form the Campbell "drift." This interpretation received some support from a Kasten core (NIWA Core Y11) collected during the site survey for Leg 181 onboard *Tangaroa* in 1996. The 2-m-long core recovered ferromanganese–stained, foraminiferal sand from the "drift" crest. The sediment was interpreted as a mixture of material reworked by the abyssal flow. Accordingly, the site was considered likely to contain a record of the abyssal circulation potentially back to the Oligocene.

Description of Lithostratigraphic Units

This lithologic sequence is divided in two units based on the visual description of the sediment and estimates of the composition from smear slides (see "Site 1121 Smear Slides," p. 19). These data are also supported by measurements of calcium carbonate, physical properties, light reflectance, and bulk mineralogy, and are summarized in Figure F3. Lithostratigraphic Unit I extends from the core top to 32.7 mbsf and is composed predominantly of terrigenous, current-influenced sediment, and is of early Pleistocene to Neogene age. Unit II contains pelagic sediment with a high biogenic component that exhibits significant variations in the dominant nannofossil and diatom constituents. Sediment of Unit II is late to early Paleocene in age and extends to the base of the core at a depth of 139.7 mbsf.

Unit I

Unit I represents terrigenous, current-influenced sedimentation and comprises Subunits IA and IB.

Subunit IA

Interval: Core 181-1121A-1H; Sections 181-1121B-1H-1 through 2H-4
Depth: 0–8.4 mbsf (Hole 1121A); 0–15.2 mbsf (Hole 1121B)
Age: early Pleistocene to pre-late Pliocene

Subunit IA is composed of alternating sediment packages. One package is composed of silty or sandy clay that is generally well bioturbated and mottled in color (Fig. F4). The sediment color ranges from yellow (10YR 7/6) to yellowish brown (10YR 5/4) to brown (10YR 7/6 and 4/4). The other sediment package contains silt, silty sand, and sand beds that are grayish brown (10YR 5/2) and light yellowish brown (10YR 6/4). The sandy bed present at the top of the core contains abundant foraminifers and nannofossils, which are not present in the sandy beds deeper within the sediment column. There is a brownish yellow (10YR 6/6) sand at the bottom of Core 181-1121B-1H that has an extremely sharp contact with the underlying yellow (10YR 7/6) clay (Fig. F5). This sand bed exhibits no grading and is not thought to be a turbidite deposit. It may represent a period of intense winnowing. A number of large ferromanganese nodules (>1 cm in diameter) are present at the core top and at three different depth horizons in Subunit IA (Figs. F6, F7). The largest nodule recovered was 7 cm long by at least 6 cm wide (Fig. F7). Ferromanganese nodules form during times of low sedimentation, yet their burial in the sediment column implies periods of either relatively higher deposition, possibly resulting from times of less erosive current activity or reduced bioturbation (McCave, 1988). Both Subunits IA and IB (0 to 32.7 mbsf) contain authigenic clinoptilolite, which suggests a significant supply of silica to the interstitial water from silica-rich material such as diatoms, radiolarians, tephras, or clays.

Subunit IB

Interval: Sections 181-1121B-2H-4 through 5X-CC
Depth: 15.2–32.7 mbsf (Hole 1121B)
Age: Between late Pliocene and late Paleocene

There is a bioturbated contact between Subunits IA and IB. This contact is also marked by a downcore decrease in the natural gamma ray and an increase in the color reflectance. Subunit IB comprises pale yellow

F3. Site 1121 summary log, p. 29.
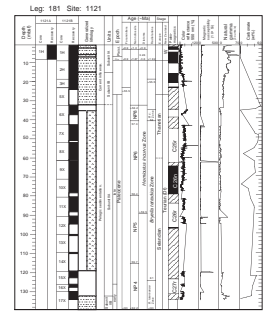
F4. Subunit IA: bioturbation, p. 30.
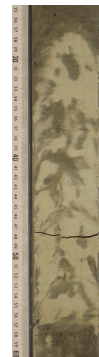
F5. Subunit IA: brownish yellow sand/yellow clay contact, p. 31.

F6. Subunit IA: ferromanganese nodules and sand, p. 32.

(2.5Y 7/4) and light yellowish brown (2.5Y 6/4) clay exhibiting faint lighter color banding and sparse black (N 1) smears, which are probably ferromanganese. Fragments of chert layers and nodules are present throughout and were responsible for the drilling difficulties, low recovery, and high core disturbance (Fig. F8). Flow-in occurs in Sections 181-1121B-2H-6 through 2H-CC and in Section 181-1121B-3H-2 to the base of the core. Cores 181-1121B-4X and 5X have poor recovery and are almost exclusively brecciated chert, which is most likely from chert layers broken by drilling and/or cave-in.

Unit II

Unit II represents a period of almost entirely pelagic, biogenic sedimentation. This unit extends from 32.7 to 139.7 mbsf and is divided into Subunits IIA and IIB, according to the relative abundance of diatoms, nannofossils, and clay in the sediment.

Subunit IIA

Interval: Sections 181-1121B-6X-1 through 17X-2
Depth: 32.7–132.7 mbsf (Hole 1121B)
Age: late to early Paleocene

Subunit IIA consists of white (10YR 8/2) nannofossil ooze that contains a subordinate amount of diatoms, radiolarians, sponge spicules, and silicoflagellates. These beds alternate with light greenish gray (5GY 7/1) nannofossil diatom ooze and greenish gray (5GY 5/2) and pale green (5G 6/2) highly diatomaceous ooze. The contact with the overlying Subunit IB was not observed because of drilling disturbance that extends through the upper part of Subunit IIA (32.7–34.2 mbsf). A single ferromanganese nodule found at the top of Core 181-1121B-6X had probably fallen downhole. Subunit IIA shows a decrease in natural gamma ray relative to Subunit IB. The top of Subunit IIA is younger than nannofossil Zone NP5 (57.5 to 58.4 Ma).

In Section 181-1121B-6X-1, at 35.07 mbsf, a sharp contact marks the change from white nannofossil ooze to light greenish gray (5GY 7/1) nannofossil diatom ooze. Until 119.4 mbsf, the sediment exhibits color variations from greenish gray (5GY 5/2), to light greenish gray (5GY 7/1), to pale green (5G 6/2) as gradational variations in Sections 181-1121B-6X-3 and 6X-4 (36.3 to 37.28 mbsf); as grayish green (5G 5/2) laminae of <1 cm thickness in Section 181-1121B-7X-5 (42.3 to 51.34 mbsf); and as color banding of greenish gray (5GY 5/2) and pale green (5G 6/2) in Section 181-1121B-8X-5 (52 to 60.06 mbsf). The lighter greenish color appears to correlate with a higher content of nannofossils while the darker green sediment represents a more diatomaceous ooze. In support, the carbonate content is substantially higher in the lighter intervals (50%) than in the darker green ooze (<10%). Bioturbation is common throughout the subunit and identified trace fossils include *Planolites* (in Sections 181-1121B-6X-3 and 6X-5), *Thalassinoides, Palaeophycus,* and *Skolithos* (in Sections 181-1121B-8X-5). The chert clasts and ferromanganese nodules that appear at the tops of Cores 181-1121B-6X, 7X, and 9X probably result from cave-in of the hole. Chert breccia and chert layers are common below 71.2 mbsf (Core 181-1121B-10X). This probably relates to the presence of diatom ooze in this depth interval. Pyrite stains are scattered throughout Cores 181-1121B-11X and 12X, and in Section 181-1121B-8X-6, gray laminae ~1 cm thick with pyritized bottom contacts are present. Moderate core dis-

F7. Subunit IA: two ferromanganese crusts, **p. 33.**

F8. Subunit IB: pale yellow clay with chert nodule, **p. 34.**
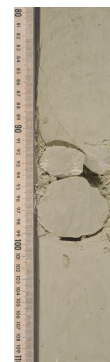
turbance is present throughout Subunit IIA and drilling biscuits appear below Core 181-1121B-11X. Recovery decreases markedly downhole with only few centimeters recovered in Cores 181-1121B-13X and 14X.

Another interval of light greenish gray (5GY 7/1) nannofossil ooze occurs between 181-1121B-15X-1 to 17X-2 (119.4-132.7 mbsf). This is interrupted by carbonate concretions and carbonate drilling breccia in Cores 181-1121-15X and 16X.

Subunit IIB

Interval: Section 181-1121B-17X-2
Depth: 132.7–139.7 mbsf (Hole 1121B)
Age: early Paleocene

The contact with Subunit IIB occurs within an interstitial water sample, and so uncertainty exists about its character and exact depth. This subunit consists of greenish gray (5GY 5/1 and 6/1) nannofossil-bearing clay. The increase in clay content is supported additionally by an increase in the natural gamma signal.

Interpretation

Site 1121 is situated on a thick sedimentary deposit close to the Subantarctic Slope of the Campbell Plateau. Both the ACC and DWBC flow along the Subantarctic Slope and influence the sedimentation in this locality.

Many characteristics of the sediment in Unit I suggest sedimentation under the presence of a vigorous, but varying, current regime. The most obvious is the very low net sedimentation rate (deposition minus erosion) of Unit I. The youngest sediment recovered at this site is late Pleistocene in age (<0.9 Ma), whereas sediments of late Paleocene age are certainly present below 33 mbsf and may be as shallow as 19.4 mbsf in Subunit IB (no datums are available between 3.6 through 56 Ma), which provides an extremely low net linear sedimentation rate (~0.6 mm/k.y.). Evidence for intervals of less or no sedimentation, reflecting the strong current influence, is given by the occurrence of ferromanganese nodules in Subunit IA. Although the sandy layer in Subunit IA has a sharp basal contact, it is not normally graded and is not thought to be turbiditic in nature. Thus, this sand layer may also document an erosional imprint of high-energy current flows with intense winnowing. The silty clay and clayey silt intervals found in Subunit IA presumably represent sedimentation under low flow conditions. Burial of ferromanganese nodules at depth within the sediment column implies that there have been episodes of higher net sedimentation. The sediment input through Unit I is predominantly terrigenous and possibly represents reworked material from Campbell Plateau or sources to the south. While it is entirely possible that turbidity currents occurred, no typical Bouma-type turbidite sequences were found.

Subunit IB comprises a relatively homogeneous clay interval, suggesting stable and low-intensity flow depositional conditions. This unit is only interrupted by the occurrence of chert layers. The age of the sequence could be late Paleocene as indicated by radiolarians (but they could be reworked), whereas no nannofossil age was available at this depth. So the existence of a hiatus between Subunits IA and IB is very likely and makes it probable that the ACC-DWBC, which is suggested to have begun during the Oligocene (Kennett, 1977), is marked by this horizon. The alternative is that the onset of the ACC-DWBC is marked

by the contact between Subunits IB and IIA following an initial high-velocity phase that eroded down to the Paleocene. Terrigenous material and biogenic silica subsequently accumulated under slower flow to form Subunit IB. Renewed current winnowing yielded Subunit IA. Distinguishing between these possibilities will require further micropaleontological work.

Unit II indicates that almost entirely pelagic, biogenic sedimentation occurred at this site throughout the early to late Paleocene. This unit has a composition similar to that inferred from nannofossil, and chert-bearing diatom ooze/fragments at DSDP Site 276 (Kennett, Houtz, et al., 1975). This succession is indicative of changes in the depth of the Carbonate Compensation Depth (CCD) through variations in presence of cold, corrosive bottom water. The top of Subunit IIA consists of nannofossil ooze with a minor amount of siliceous fossils, and was probably deposited above the paleo-CCD. The sharp contact with the underlying diatom-rich sediment, concurrent with a slight decrease in nannofossil content, was possibly caused by a shallowing of the CCD. The increased content of nannofossils in Cores 181-1121-15X to 17X suggests a relatively deeper CCD between ~60 and 62 Ma. Subunit IIB is mostly depleted of nannofossils, which may reflect deposition below the CCD. The high clay content of this unit is confirmed by the higher gamma-ray signal in this depth interval.

Discussion and Conclusion

Although Hole 1121B initially penetrated the drift-type silty sediment characteristic of Unit I, the presence of Paleocene siliceous and calcareous pelagites in the rest of the sequence shows that the main sediment body is not a drift, as suggested by Carter and McCave (1997). Rather, it now appears to be the remnant of a pelagic apron that formed along the eastern margin of Campbell Plateau. Subsequent initiation of a strong abyssal circulation under the ACC and DWBC has extensively eroded the apron. Apart from Unit 1, the post-Paleocene succession has been either eroded or prevented from accumulating or both these processes have occurred. Furthermore, topographically induced scour along Campbell Plateau has effectively isolated the apron sediment to produce a linear sediment body on the floor of the adjacent Southwest Pacific Basin.

From a paleoceanographic perspective, there have been several bouts of current activity, the precise ages of which are yet to be delineated. The initial phase(s) of strong bottom flow resulted in erosion of the apron. Until more drill-hole information is available from the Oligocene through Miocene interval, we can only speculate that these phases coincided with the late Oligocene opening of the circum-Antarctic seaway and a late Miocene cooling event in Antarctica (e.g., Kennett, 1977). Both these events would have encouraged the production and passage of deep waters through the Southwest Pacific, and produced widespread unconformities, manifested by including seismic reflectors X and Y of Kennett, von der Borch, et al. (1986). In addition, the presence of at least three ferromanganese nodule/sand horizons in Subunit IA also suggests periods of strong current activity, occasionally punctuated with periods of quieter currents and therefore more sediment accumulation. Assuming the youngest sediments are late Pleistocene in age, it then appears that strong erosive currents have prevailed since that time. Assessments of the sedimentary regime of southern New Zealand (Carter and McCave, 1997) and physical oceanographic observations

coupled with the output from a numerical model (Carter and Wilkin, in press) reveal that the dominant force behind abyssal erosion along the front of the Campbell Plateau is the ACC. Interaction of the current with the marked topography of Campbell Plateau intensifies the flow as well as forming large-scale eddies that extend from the surface to the seabed (Bryden and Heath, 1985; Morrow et al., 1992).

Implications for the Eastern New Zealand Oceanic Sedimentary System

The discovery of extensive erosion off Campbell Plateau allows us to refine the model for the Eastern New Zealand Oceanic Sedimentary System (ENZOSS). When first proposed, it was suggested that some of the sediment transported north by the ACC-DWBC accumulated on what was interpreted as the Campbell "drift," with another portion moving east with the ACC (Carter et al., 1996). The cores recovered from Site 1121 show that very little sediment settled in this region. For example, the layer of drift sediment capping the oceanic Paleocene sediments is, at most, only 32.7 m thick, and it may be as little as 15.2 m. It would appear that the ENZOSS system to the south of Bounty Fan (i.e., within the path of the ACC) is dominated by erosion and transport. North of the fan, erosion is less pervasive and sediment accumulates as drifts (McCave and Carter, 1997).

BIOSTRATIGRAPHY

Introduction and Summary

The uppermost sediments at Site 1121 are current-influenced silty clays and sands with frequent manganese nodules. The sediments contain both calcareous and siliceous microfossils of late Pleistocene to late Pliocene age (Figs. **F9, F10**). The underlying sediments, which represent a late early to late Paleocene age, are nannofossil-diatom oozes and siliceous clays with porcellanite and chert layers in the deeper part (Fig. **F9**). All major microfossil groups, including calcareous nannofossils, diatoms, radiolarians, and benthic foraminifers, are present and extremely well preserved. The highly diverse assemblages provide an integrated biostratigraphy to combine with the magnetostratigraphy, which for the first time provides a continuous pelagic Paleocene record for the Southwest Pacific Ocean.

A significant hiatus (Fig. **F9**) between Samples 181-1121A-1H-CC and 181-1121B-2H-CC (8.32–19.4 mbsf) in Site 1121 represents a long age gap between the early late Pliocene and the late Paleocene (~53 Ma). Using our best fit from the constraining datum levels from all four microfossil groups, we conclude that Site 1121 cored a very thin sediment drift between 0 and 3 mbsf. A detailed diatom analysis indicates that the topmost part (0–0.36 mbsf) is of late Pleistocene age (<0.42 Ma), and the interval between 0.36 and 0.90 mbsf is probably of early Pleistocene age (0.65–1.8 Ma). A late Pliocene age (2.2–3.36 Ma) was determined for the short interval between 0.90 and 1.00 mbsf and an early Pliocene age (3.26–3.6 Ma) between 1.00 and 3.00 mbsf.

The stratigraphic sequence recovered at Site 1121 is a nearly complete section of late early to late Paleocene-age sediments (56 to 62 Ma). The sequence (32.72–134.72 mbsf) can be correlated with four nannofossil zones (NP8 to NP4), three radiolarian zones (RP6 to RP4), and one

F9. Biostratigraphic summary chart, **p. 35.**
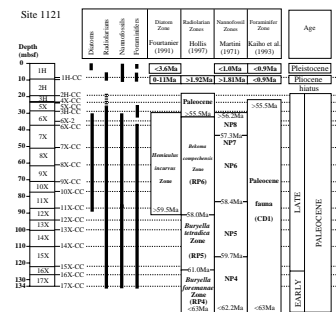
F10. Age assignments based on planktonic diatoms, **p. 36.**
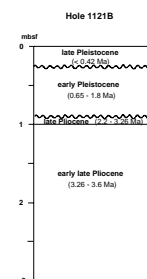
diatom zone, respectively (Fig. F9). The correlation and age assignments between diatoms, radiolarians, calcareous nannofossils, and foraminifers are strongly concordant. From our analysis, the boundary between lower and upper Paleocene is placed at a horizon between Samples 181-1121B-15X-CC and 16X-CC (122.30–127.20 mbsf). Stratigraphically useful datum levels such as FOs of *Heliolithus kleinpelli* (base of NP6 in Sample 181-1121B-10X-CC), *Fasciculithus tympaniformis* (base of NP5 in Sample 181-1121B-14X-CC), and *Buryella tetradica* (base of RP5 in Sample 181-1121B-15X-CC) are also recognized.

Age

The micropaleontological biostratigraphy of Site 1121 is based mostly on the onboard study of core-catcher samples. Hole 1121A samples were used for the uppermost part of the section and Hole 1121B samples for the lower part. Additional samples were taken from within selected cores to address specific age and paleoenvironmental questions. The absolute ages assigned to biostratigraphic datums follow the references listed in Tables T2, p. 59, T3, p. 60, T4, p. 63, T5, p. 64, all in the "Explanatory Notes" chapter.

Calcareous Nannofossils

The nannofossil assemblages from the uppermost part of Holes 1121A and 1121B (from the core top to Sample 181-1121B-5X-CC) are extremely poor, and several samples are totally barren. We examined many samples from the upper part of the first core, but the scarcity of nannofossils made the sediments difficult to date. However, based upon the occurrence of *Gephyrocapsa parallela* (originated at about 0.95 Ma), the very top of the section is late Pleistocene in age. Downcore, from Sample 181-1121B-1H-CC to 5X-CC (8.32–23.72 mbsf), a few late Neogene nannofossils occur and indicate an age older than Pleistocene, based upon the absence of typical Pleistocene *Gephyrocapsa* species.

Nannofossils are generally abundant and moderately preserved in Cores 181-1121B-6X to 17X (Table T2). An apparently complete middle Paleocene section (lower Seladian Stage and upper Danian; Zones NP4 to NP8 of Martini, 1971) was recovered. Species of high latitudes, such as those of *Prinsius, Chismolithus, Hornibrookina,* and *Toweius* are abundant. Differential dissolution, however, has resulted in the destruction of the central parts of many specimens, which renders species identification difficult. The stratigraphic distribution of the identifiable species is presented in Table T2.

Datum levels belonging to the *Fasciculithus-Bomolithus-Heliolithus* group were recognized, which allowed us to correlate Cores 181-1121B-6X to 17X to NP8–NP4. The topmost two sections of Core 181-1121B-6X are characterized by the unique occurrence of *Fasciculithus bobii* and *Heliolithus redelii*. The association of these two species suggests strongly that these two sections are correlated to Zone NP8. The occurrence of *Bomolithus elegans* in Sample 181-1121B-6X-1, 2 cm, further constrains that the uppermost part of Core 181-1121B-6X is in the middle to lower part of Zone NP8 (Perch-Nielsen, 1985). Furthermore, based upon the first appearance of *F. bobii* in Sample 181-1121B-6X-CC, we assigned the bottom of Zone NP8 to Core 181-1121B-7X.

The next easily recognized datum is the first occurrence of *Heliolithus kleinpellii* in Sample 181-1121B-10X-CC, which marks the base of Zone NP6. It is not possible to define the NP7 biozone, because of the lack of

T2. Identification and abundance of nannofossils, p. 56.

the marker species *Discoaster mohleri* at the base of Zone NP7. Consequently, Cores 181-1121B-7X-CC to 10X-CC are assigned to the Zones NP6–NP7.

The first occurrence of the marker species of the base of Zone NP5, *Fasciculithus tympaniformis,* was observed in Sample 181-1121B-14X-CC. The first occurrence of the continuous occurrence of *Sphenolithus primus* in Core 181-1121B-14X also supports the placement of the NP5/NP4 boundary below Core 181-1121B-14X. The occurrence of *Fasciculithus janii* and *F. ulii* in the lowermost cores (Cores 181-1121B-15X, 16X, and 17X) is consistent with the known evolutionary succession of this genus (Perch-Nielsen, 1985). The occurrence of these two species also indicates that the bottom of Hole 1121B is in the topmost part of Zone NP4.

Foraminifers

The top meter below seafloor (down to Sample 181-1121A-1H-1,18–20 cm) contains rich calcareous, foraminiferal faunas, which become progressively less abundant downhole. Planktonic forms compose over 99% of the foraminifers and are dominated by white *Globigerina bulloides, Globorotalia inflata,* and small *Neogloboquadrina pachyderma,* with fewer *Globorotalia truncatulinoides* and *Globigerina quinqueloba*. These suggest a late Pleistocene to Holocene age (<0.9 Ma). Horizons within this upper interval (e.g., Sample 181-1121A-1H-1, 0–1 cm) and below (down to Sample 181-1121B-1H-CC) contain a much reduced foraminiferal fauna, lacking small specimens and only containing sparse large, thick-walled, white *Globorotalia inflata* and *Globigerina bulloides,* together with isolated *Globorotalia truncatulinoides* and benthic foraminifers. This relict, current-sorted, and partly dissolved assemblage is still likely to be of late Pleistocene age (<0.9 Ma).

From Samples 181-1121B-1H-CC to 13X-CC, the only microfossils recovered were radiolarian casts, sponge spicules, and fish teeth (e.g., in Sample 181-1121B-5X-CC), with the exception of Sample 181-1121B-3H-CC, which contains an impoverished agglutinated benthic foraminifer assemblage with frequent specimens of *Rzehakina epigona* and *Spiroplectammina spectabilis,* and rare *Rhabdammina* sp. and *Tritaxia* sp. This assemblage is Paleocene in age, in agreement with the more diverse assemblage, including the same taxa, deeper in the hole. Sample 181-1121B-6X-2, 60–65 cm, proved to be barren.

In Hole 1121B samples, a more diversified Paleocene foraminiferal assemblage was recovered in and below Core 181-1121B-11X (Table T3). The most abundant and best preserved faunas occur in Samples 181-1121B-15X-CC and 16X-CC. Identified taxa include (recorded New Zealand time ranges in brackets, from Hornibrook et al., 1989): *Spiroplectammina spectablis* (Late Cretaceous–Paleocene), *Hormosina ovulum ovulum, Cribrostomoides trinitatensis, Glomospira charoides, Reticulophragmium* aff. *paupera, Rzehakina epigona* (Cretaceous–Paleocene), *Rhabdammina* sp., *Psammosphaera* sp., *Arenobulimina* aff. *dorbignyi, Dorothia* aff. *oxycona, Dorothia* spp., *Tritaxia* sp., *Conotrochammina whangaia* (Late Cretaceous–Paleocene), *Alabamina creta* (latest Cretaceous–Paleocene), *Allomorphina conica* (late Paleocene–middle Eocene), *Anomalinoides piripaua* (Late Cretaceous–Paleocene), *Charltonina acutimargina* (latest Cretaceous–Paleocene), *Nuttallides carinotruempyi* (late Paleocene–middle Eocene), *N. florealis* (late Paleocene, Sample 181-1121B-16X-CC), *Oridorsalis umbonatus, Gavelinella beccariiformis* (latest Creta

T3. Identification and abundance of foraminifers, **p. 57.**

ceous–Paleocene), *Pullenia bulloides, Valvulineria teuriensis* (latest Creta-
ceous–Paleocene), and *Lenticulina* spp.

The assemblage may be assigned a Paleocene, probably middle to late
Paleocene age (late Teurian Stage, ~62–55 Ma) or within deep-sea
benthic zone CD1 (older than 55.5 Ma, Kaiho et al., 1993).

Diatoms

In Hole 1121B, diatoms are present and well preserved in the top 3 m
of Core 181-1121B-1H and throughout Cores 181-1121B-6H to 11X
(Table T4; Fig. F10). In the interval between (Core 181-1121B-1H-3 to
Core 5H), and below (Core 181-1121B-12X), silica diagenesis has
destroyed the original diatom content, and the authigenic zeoliths cli-
noptilolite and phillipsite are present instead.

The upper 3 m of this site contains Neogene diatom assemblages, in
which from the top down a sequence of Pleistocene and then Pliocene
species associations can be recognized (Fig. F10), with more rare, clearly
reworked Miocene species admixed. The frequent to common occur-
rence of *Hemidiscus karstenii,* together with a typical late Pleistocene
diatom assemblage, indicates an age younger than 0.42 Ma for the
upper 36 cm of the core. Below, the most abundant species are charac-
teristic of the early Pleistocene and Pliocene, such as *Thalassiosira ellipti-
pora, T. vulnifica, T. inura, T. kolbei, T. insigna, Simonseniella barboi,
Nitzschia weaveri, N. praeinterfrigidaria,* and *N. interfrigidaria;* species that
ranged into the early Pleistocene such as *Nitzschia barronii* and *Actinocy-
clus karstenii* also occur. Although the assemblages contain several spe-
cies that do not occur with overlapping stratigraphic ranges,
nevertheless, some of the younger species are delimited to the upper
part of this core, so that a sequence to successively older species can be
constructed. An example of a relatively young species that occurs only
in the upper part of the diatom-containing Neogene is *Thalassiosira
elliptipora,* which ranges from 0.65 to 1.8 Ma. This species is not found
below Sample 181-1121B-1H-1, 89–90 cm. It therefore is used as an
argument to place the core interval from 36 to 90 cm into the lower
Pleistocene.

Another species with an occurrence restricted to the upper part of the
section is *T. vulnifica* (stratigraphic range 2.2–3.26 Ma). It was not found
below Sample 181-1121B-1H-1, 100–102 cm, suggesting a late Pliocene
age for core between 0.9 and 1 mbsf. Below 1 mbsf, reworked Miocene
species like *Hemidiscus ovalis, H. karstenii* f. 1, *Bruniopsis mirabilis, Dentic-
ulopsis hustedtii, D. dimorpha, D. meridionalis,* and *Nitzschia denticuloides*
are more common in association with an otherwise early late Pliocene-
age diatom assemblage. This core interval from 1 to 3 mbsf is placed,
because of the absence of *T. vulnifica* and the presence of the other
above-listed Pliocene species, into an age range from 3.26 to 3.6 Ma.

The upper 3 mbsf, interpreted as drift deposits, is thus documenting
slow sedimentation rates of 0.1 to 0.5 cm/k.y. in the late Neogene, with
the intervals of preserved sediment separated by two hiatuses, and the
deposits characterized also by the presence of reworked Miocene micro-
fossils.

The well-preserved, diverse Paleocene diatom assemblage from Cores
181-1121B-6X to 11X fall into the *Hemiaulus incurvus* Zone of Four-
tanier (1991). The marker species that delimits this zone (top *Tricera-
tium gombosi;* bottom *Hemiaulus peripterus*) were not found during
shipboard analysis. *T. gombosi* is a very small species, and a good separa-
tion of the diatoms from the sediment matrix was not possible during

T4. Identification and abundance
of diatoms, p. 58.

shipboard preparation, but may be possible during shore-based analysis.

Radiolarians

The radiolarian biostratigraphy at Site 1121 is based on the examination of 20 core-catcher samples and two core samples (Table T5). The top core sample (181-1121A-1H-1, 0–2 cm) contains rich radiolarian faunas including abundant *Spongoplegma antarcticum* and *Cycladophora pliocenica* together with rare *Antarctissa denticulata, Antarctissa strelkovi, Lithelius nautiloides* (FO 1.93 Ma), and common *Eucyrtidium calvertense* (LO 1.92 Ma). The radiolarians indicate older than latest Pliocene age (>1.92 Ma). The other core-catcher samples near the top (181-1121A-1H-CC, 181-1121B-1H-CC, 1–3 cm, 181-1121B-1H-CC, 6–8 cm, and 181-1121B-1H-CC) are barren or very rarely contain radiolarians.

Sample 181-1121B-2H-CC contains very rare specimens of *Amphipyndax stocki* (Early Cretaceous–Paleocene), *Myllocercion acineton* (Late Cretaceous–Paleocene), and *Amphisphaera* sp. Sample 181-1121B-3H-CC yields rare but age-diagnostic specimens of *Amphisphaera goruna* (early Paleocene to early Eocene), *Buryella tetradica* (FO 61 Ma, Hollis, 1997), *Lithomespilus coronatus* (Late Cretaceous to early Eocene), and *Rhopalocanium* aff. *ornatum.*

Sample 181-1121B-4X-CC includes rare *Amphisphaera kina,* indicating an early to late Paleocene age. In Sample 181-1121B-5X-CC radiolarians are absent, but fish teeth are commonly observed. These assemblages are late Paleocene in age, which is concordant with the age assignments for the deeper samples.

Radiolarian faunas from Samples 181-1121B-6X-CC to 17X-CC are generally well preserved and highly diversified, with the exception of Samples 181-1121B-12X-CC to 14X-CC, which contain lithologies like chert or hard siliceous hemipelagic limestone. However, these faunas give an excellent, continuous record of an early to late Paleocene oceanic history. Throughout this radiolarian-rich interval, *Amphisphaera coronata* s.l., *Amphisphaera goruna, Bathropyramis sanjoaquinensis* s.l., and *Spongodiscus* sp. are present. In addition, common occurrence of *Buryella tetradica,* rare to common *Buryella* cf. *tetradica,* and rare to common *Buryella granulata* characterizes this interval. *Corythomelissa adunca* has a rare to few occurrence, which also characterizes the fossiliferous section (Samples 181-1120B-6X-2, 60–65 cm, to 11X-CC). Abundant *Microsciadiacapsa* sp. is present in Samples 181-1121B-7X-CC and 11X-CC. Rare to few *Buryella foremanae* are consistently present in the lowest Sections 181-1121B-15X-CC to 17X-CC.

The first occurrence (FO) of *Buryella tetradica,* which marks the base of the *Buryella tetradica* Zone (RP5), is placed between Samples 181-1121B-15X-CC and 16X-CC. According to the Cretaceous–Paleocene radiolarian study in New Zealand by Hollis (1997), the interval 181-1120B-6X-2, 60–65 cm, to 11X-CC (34.8–87.1 mbsf) can be assigned to the *Bekoma compechensis* (RP6) Zone (58.0–55.5 Ma), interval 11X-CC to 15X-CC (87.1–122 mbsf) to the *Buryella tetradica* (RP5) Zone (58–61 Ma), and the lowest interval 16X-CC to 17X-CC (122–134 mbsf) to the *Buryella foremanae* (RP4) Zone (61–63 Ma), respectively (Fig. F9). Although *Bekoma compechensis,* a nominal species of the Zone RP6, could not be identified, *Corythomelissa adunca,* which first appears in the lower part of the RP6 Zone (Hollis, 1997), was found in Samples 181-1120B-6X-2, 60–65 cm, to 11X-CC. It is noteworthy that the FO of *Buryella* cf. *tetradica* (three-segmented form) is recognized in Sample

181-1121B-15X-CC and then the FO of *Buryella tetradica* s.s. (four-segmented form) is recorded in Sample 181-1120B-11X-CC.

Paleoenvironment

Backtracking and Paleoceanography

Site 1121, at the foot of the Campbell Plateau, was drilled in the vicinity of marine magnetic anomaly 32, in 4511 m present-day water depth. The present-day CCD is near 4700 m. Using generalized backtracking by assuming a normal or slightly shallow ocean spreading-ridge crest in Late Cretaceous time (late Campanian), and 1 km of Campanian–Paleocene sediment accumulation, a probable paleo–water depth of ~ 3500 m is indicated at Site 1121 in the mid-Paleocene (Fig. F11). Previous estimates of the Late Cretaceous through Cenozoic CCD in the Pacific (Van Andel, 1975; Kennett, 1982) indicate a Paleocene CCD depth just below 3000 m. Hence, Site 1121, in Paleocene time, probably was at or just below the CCD. These data are in agreement with the finding that Paleocene planktonic foraminifers have been dissolved, whereas Paleocene nannofossils are only partly dissolved, and do occur in smear-slide residues. Agglutinated foraminifers, resistant to dissolution, are common. Apparently, in Paleocene time, ODP Site 1121 was located at a paleo–water depth between the CCD for nannofossils and planktonic foraminifers. As may be seen from Figure F11, Site 1121 was above the CCD in the early Paleocene, in agreement with the fact that calcareous benthic foraminifers, and a relatively high proportion of ataxophragmiid agglutinated taxa with calcareous cemented tests, were preserved in the oldest three cores above the bottom of the hole. The unknown variables are the properties of Cretaceous ocean crust that might produce an anomalously shallow or deep ridge, and the precise location of the CCD in the vicinity of a noncarbonate continental margin (i.e., New Zealand) in a relatively warm ocean.

Foraminifers

The young foraminiferal fauna from the upper unit in the hole (Core 181-1121B-1H) is typical of shallow abyssal environments close to the CCD. The upper samples with rich faunas contain a mix of fresh large and small planktonic forms that were rapidly buried and preserved, together with many broken and partly dissolved larger, thicker-walled tests that spent longer on the seafloor before being buried. This dissolution is indicated by the 2:1 ratio of planktonic test fragments/whole tests. Horizons with more depauperate faunas only retain the thicker-walled, larger, dissolution-resistant tests, and these intervals presumably had a lower sedimentation rate.

The impoverished agglutinated foraminiferal assemblage recovered from the Paleocene interval at Site 1121 is part of the cosmopolitan assemblage that is widespread worldwide in bathyal to shallow abyssal continental margins and in abyssal plains from the Late Cretaceous to the Paleogene (Gradstein and Berggren, 1981). The common presence of calcareous benthic foraminifers and of ataxophragmiid agglutinated taxa with calcareous cemented tests in several core-catcher samples indicates limited dissolution of tests below the local CCD. On the other hand, the marine pelagic "snow" from planktonic foraminifers was dissolved before landing on the ocean floor. That common to abundant planktonic forms might have been expected with a deeper CCD, or

F11. Tentative model of oceanic crust subsidence and CCD history, p. 37.
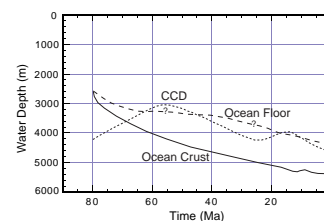
shallower site setting, is known through drilling of DSDP Site 277 (80% planktonic foraminifers in the upper Paleocene; Hollis et al., 1997), in 1214 m present-day water depth on the western edge of the Campbell Plateau.

In composition, the Site 1121 Paleocene fauna appears to be an impoverished version of the rich and diverse deep-water assemblage of the type Teurian and the Tawanui sections (Whangai facies) on the East Coast of the North Island of New Zealand (Hornibrook et al., 1989; Kaiho et al., 1993). The benthic fauna of Site 1121 has much in common with the impoverished assemblage recorded from the gray silt-stone and limestone unit above the ribbon chert unit of middle to late Paleocene age in Marlborough, northern South Island (Strong et al., 1995), and the late Paleocene assemblage from nearby DSDP Site 277, except for the lack of planktonic forms (Hollis et al., 1997).

The Site 1121 Paleocene foraminiferal fauna differs significantly from:

1. The agglutinated Paleocene assemblages (dominated by *Cyclammina elegans* and species of *Budashevaella, Ammodiscus, Ammobaculites,* and *Haplophragmoides*) that are interpreted to have accumulated in silled, anoxic, shallow-water basinal conditions in North Otago (Hornibrook et al. 1989);
2. The agglutinate-dominated Paleocene assemblages (dominated by *Cyclammina elegans, Budashevaella* spp., and *Haplophragmoides*) that are interpreted to have accumulated at shelf depths in the adjacent Great South Basin (Raine et al. 1993); and
3. The planktonic-bearing, calcareous benthic foraminiferal fauna (dominated by species of Lagenidae, *Patellina, Rosalina,* and *Cibicides*) from Red Bluff Tuff, Chatham Island, that is interpreted as having accumulated in normal marine conditions at outer shelf to upper bathyal depths (Campbell et al., 1993).

Diatoms and Silica Diagenesis

During the late Neogene and Quaternary subantarctic/Antarctic, fully planktonic species were deposited at this site. During the middle Paleocene, the assemblages are dominated by cosmopolitan, neritic species, which may have been transported downslope from the Chatham Plateau area. The abundance of siliceous microfossils, especially of the most abundant group among them, the diatoms, is inversely correlated to the abundance of the authigenic zeolites clinoptilolite and phillipsite (Fig. F12). The interval of well-preserved middle Paleocene diatomaceous clayey silts is flanked above and below by sediments strongly affected by silica diagenesis. Silica diagenesis here has not only resulted in dissolution of biogenic silica and precipitation of zeolites, but also in the formation of chert nodules and chertified layers.

Radiolarians

The Pliocene radiolarian fauna from Sample 181-1121A-1H-1, 0–2 cm, consists of diversified species of typical Antarctic/subantarctic environments (e.g., *Antarctissa denticulata, Antarctissa strelkovi,* and *Spongoplegma antarcticum*).

The early to late Paleocene radiolarian succession recognized in Hole 1121B has excellent preservation with highly diversified faunas. The succession's thickness (RP6 Zone: 34.8–87.1 mbsf, RP5 Zone: 87.1–122

F12. Relative abundance of diatom valves, **p. 38.**
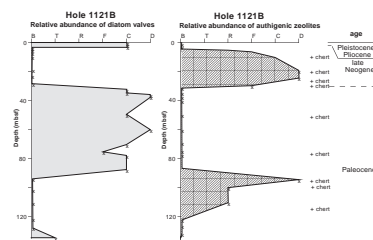
mbsf, RP4 Zone: 122–134 mbsf) is similar to or greater than the age-equivalent units of the Mead Stream section (RP5 + RP4 Zones: ~50 m thick) and Woodside Creek section (RP5 + RP4 Zones: ~30 m thick) in the Marlborough area of South Island, New Zealand (Hollis, 1997; Strong et al., 1995).

PALEOMAGNETISM

Core archive-halves from Hole 1121B were measured on the shipboard pass-through cryogenic magnetometer. Declination, inclination, and intensity of natural remanent magnetization (NRM) were routinely measured at 5-cm intervals at 10- and 20-mT alternating field (AF) demagnetization steps. In situ Tensor tool data were not collected as only three APC cores were collected before refusal, and coring continued with the XCB method. Therefore, only inclination could be used to determine the magnetic polarity of Hole 1121B. At least two oriented discrete samples were collected from the working half of each core interval for progressive AF and thermal demagnetization and rock magnetic studies. Whole-core magnetic susceptibility was measured routinely on all cores, using a Bartington susceptibility loop on the automated multisensor track (MST).

Magnetic properties vary with lithology downcore (Fig. F13). In lithostratigraphic Subunit IA (0–15.2 mbsf), a bioturbated, yellowish brown, silty and sandy clay, NRM intensities mimic susceptibility and are relatively high (about 10^{-2} A/m and about 10^{-4} SI volume units, respectively). Beneath a sharp contact, Subunit IB (15.2–32.7 mbsf, pale yellow clay) has much lower NRM intensities (about 10^{-4}–10^{-5} A/m on average), but susceptibility remains moderately high (10^{-5} SI). Susceptibility and NRM intensities are both low (10^{-6} SI and 10^{-4}–10^{-5} A/m, respectively) in Unit II, a mostly light green pelagic diatomaceous ooze (32.7–134.5 mbsf, base of hole).

Paleomagnetic Behavior and Rock Magnetism

Lithostratigraphic Unit I

In the upper 28 m of the core, NRM measurements displayed consistent, steeply positive (downcore) inclinations ranging between +70° and +80°, consistent with a drill-string overprint induced during coring. The 20-mT AF demagnetization step proved very effective in removing the overprint and revealing a well-defined polarity reversal stratigraphy (Fig. F14). Intensity of magnetization in lithostratigraphic Unit I was strong enough to subject discrete samples to stepwise AF demagnetization of up to 80 mT in the shipboard pass-through cryogenic magnetometer. In each case, the drilling-induced overprint accounted for 30%–80% of the NRM but was removed by the 10-mT step of demagnetization (Fig. F15). Further stepwise AF demagnetization was mostly effective in isolating a primary remanence direction, but the signal was generally noisy (Fig. F15). A single sample (26.04 mbsf, Fig. F15D), taken from the interval of "flow-in" from within Subunit IB, had a horizontal drilling-induced overprint but moderate inclination upon cleaning. Steep paleomagnetic inclination has been reported to distinguish "flow-in" from other intervals of core (e.g., Roberts et al., 1996); however, inclination was not distinctly different in this case. After AF cleaning, selected discrete samples from Unit 1 were subjected to progressive

F13. Whole-core magnetic susceptibility and NRM measurements, **p. 39.**
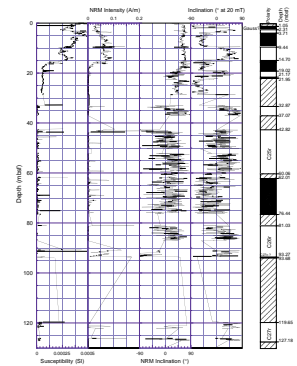
F14. MS and NRM from the upper 25 mbsf of Hole 1121B, **p. 40.**
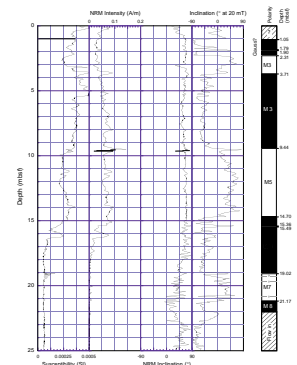
F15. Vector component and equal area diagrams, **p. 41.**
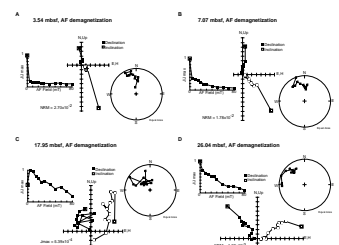
isothermal remanent magnetization (IRM) fields until saturation (Fig. F16A). Magnetization was "soft" and samples were generally saturated by 200 mT, although some samples did not saturate fully until 500 mT. Coercivity of remanence (B_{cr}) was less than 50 mT in all samples. AF and thermal demagnetization of the saturation IRM (SIRM) shows two components of magnetization with overlapping coercivity and blocking temperature spectra (Figs. F17A, F17B, F17C). The lower blocking temperature component is removed by 300°–400°C and the high-temperature component remains until 580°–600°C, although a very minor component may persist above 600°C.

The "soft" SIRM, low B_{cr}, and distributed unblocking temperatures up to 580°–600°C demonstrate that multiple grain–size magnetite is the main carrier of remanence in samples from Unit I. However, a small component of remanence may be held by a sulfide mineral, such as pyrrhotite, which would explain slightly harder IRM acquisition curves and higher values of saturation magnetization for some samples (Fig. F16A), as well as the low unblocking temperature component of SIRM in all samples (Fig. F17). The presence of sulfides may also explain why AF demagnetization of NRM produces noisy results (e.g., Fig. F15C) as pyrrhotite is known to respond poorly to AF demagnetization methods (e.g., Turner and Kamp, 1990; Roberts and Turner, 1993; Wilson and Roberts, 1999).

Lithostratigraphic Unit II

The NRM inclination record in Unit II is very noisy and not obviously overprinted by the drilling process. This is most likely a result of the very low intensity of magnetization throughout Unit II. The 20-mT AF demagnetization step is still noisy; however, it is possible to distinguish intervals of dominantly positive vs. intervals of dominantly negative inclination. Because of the low intensities of magnetization and poor response to AF cleaning of archive core halves on the shipboard pass-through cryogenic magnetometer, further AF cleaning of discrete samples was not attempted, but several discrete samples were given an IRM. Typical IRM and backfield IRM acquisition curves are shown in Figure F16B. Sample magnetizations are "harder" than those from Unit I and did not saturate until applied fields of 500–1000 mT. B_{cr} values were between 75 and 100 mT. Alternating-field demagnetization to 60 mT only removed 50% of the SIRM. Thermal demagnetization of the SIRM shows two components of magnetization with overlapping blocking temperature spectra (Figs. F17D, F17E, F17F). The lower unblocking temperature component is again removed by 300°– 400°C, but it is a more prominent component in Unit II than it was in Unit I. The high-temperature component persists until 580°–600°C, except in one case where it persists to 680°C (Fig. F17F).

The "harder" SIRM and higher B_{cr} in Unit II suggests that an iron sulfide mineral (possibly pyrrhotite) is more dominant in holding remanent magnetization than it was in Unit I. However, even though less dominant, magnetite of multiple grain sizes is still present, as demonstrated by the distributed higher-temperature unblocking spectra that generally persist until 580°–600°C (Figs. F17D, F17E, F17F). A minor component of magnetization may once again persist to higher temperatures in a few samples. This is most likely to be caused by hematite from rust contamination during the drilling process. Unblocking temperature spectra in Figure F17 clearly show that the lower blocking temperature spectra component is more dominant in Unit II (Figs. F17A, F17B,
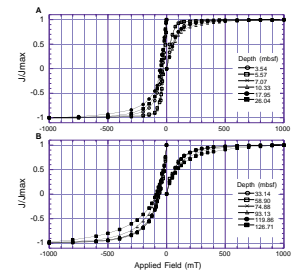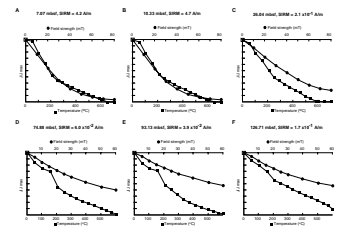
F17C) than in Unit I (Figs. F17D, F17E, F17F). The dominance of pyr-rhotite may well explain the low NRM intensities for Unit II, the lack of a drilling-induced overprint component to the NRM, and the ineffectiveness of AF demagnetization in isolating a clear primary inclination pattern for Unit II. It is possible that the AF demagnetization was only effective in removing any drilling-induced component of the NRM in Unit II.

Magnetostratigraphy

Lithostratigraphic Unit I

Tensor tool data were not collected in core from Hole 1121B because of early APC refusal, so only inclination could be used to determine polarity. In Unit I, after 20 mT of demagnetization, the inclination pattern allows a clear determination of magnetic polarity stratigraphy for the upper 22 mbsf of the drill hole (Fig. F14). Four major normal polarity magnetozones were identified (M2, 1.05–2.31 mbsf; M4, 3.71–9.44 mbsf; M6, 14.70–19.02 mbsf; and M8, 21.17–22.00 mbsf). Polarity could not be unambiguously determined in the uppermost meter of Hole 1121B, probably because this interval comprises saturated, unconsolidated, well-sorted, medium sand. However, it is possible that this is an interval of reversed polarity. Polarity could also not be determined for the lowermost part of Unit I because of a combination of "flow-in" during coring and loss of recovery. A Pliocene diatom assemblage was recovered from the top 3 m of Hole 1121B (see "Biostratigraphy," p. 8). Based on this, the uppermost normal polarity interval (1.05–2.31 mbsf) is tentatively correlated with the lower part of the Gauss magnetochron of the Geomagnetic Polarity Time Scale (GPTS) (Berggren et al., 1995; Cande and Kent, 1995). This correlation would imply that at 2.3 mbsf the sediments are already 3.6 Ma old and either the uppermost part of the hole is very condensed, or the Pleistocene is not recorded at Site 1121. The frequent polarity reversal pattern within Unit I (Fig. F14) also suggests quite slow sedimentation rates and a condensed record. Unfortunately, no biostratigraphic information is available to assist with correlation of any of the magnetozones in Subunit IB to the GPTS, and the magnetic polarity pattern is not unique and cannot be correlated independently. Furthermore, several disconformable horizons are identified where time may be missing (see "Lithostratigraphy," p. 3). However, only the reversal boundary between M6 (normal) and M7 (reversed) occurs in a lithostratigraphic break marked by a chert bed; all other reversal boundaries do not appear to occur in lithostratigraphic breaks.

Lithostratigraphic Unit II

A major lithostratigraphic disconformity is noted between Units I and II. Diatoms, radiolarians, nannofossils, and foraminifers recovered from Unit II are confined to the Paleocene and confirm a major unconformity in the vicinity of the chert horizons in Cores 181-1121B-3H, 4H, and 5H (19.0–32.7 mbsf, see "Biostratigraphy," p. 8). In Unit II, the inclination signal is noisy, because of the ineffectiveness of AF demagnetization, and the polarity record disjointed by the many intervals of poor or no recovery. Despite this, four distinct polarity zones can be identified (Fig. F13): a reversed-normal-reversed polarity sequence between 42.82 and 93.27 mbsf, and an interval of reversed polarity

between 119.65 and 127.18 mbsf. All reversal boundaries lie within unrecovered intervals at core breaks, except for a possible transition to normal polarity at 93.27 mbsf at the base of the reversed-normal-reversed (R-N-R) sequence (Fig. F13). Radiolarian zones (*Bryella tetradica,* RP5, and *Bekoma compechensis,* RP6) and nannofossil zones (NP5–NP8) allow direct correlation of the R-N-R sequence with Chrons C26r-C26n-C25r (see "Biostratigraphy," p. 8) (Fig. F18). The combination of the *Bryella foremanae* (RP4) radiolarian zone and the nannofossil NP4 zone beneath 120 mbsf suggests that the reversed polarity zone (119.6–127.18 mbsf) in the lower part of the hole must correlate with part of Chron 27r of the GPTS. If the polarity reversal at 93.27 mbsf is real, it must by definition correlate with the top of C27n of the GPTS. However, this is in disagreement with the nannofossil zone (NP5) throughout this interval (see "Biostratigraphy," p. 8). Because it occurs just above an interval of nonrecovery, more detailed work is necessary to be sure polarity has been correctly identified. Correlation with the GPTS is well constrained by biostratigraphic datums and suggests sedimentation rates of about 15 m/m.y. for the Paleocene interval in Hole 1121B (about 40–130 mbsf), as opposed to much lower sedimentation rates at the top of Hole 1121B (possibly about 1 m/m.y.). Thermal demagnetization will be undertaken on discrete samples from the Paleocene interval of Hole 1121B to confirm and better define the polarity stratigraphy reported here from shipboard studies.

AGE MODELS AND SEDIMENTATION RATES

Biostratigraphic levels with age significance at Site 1121 were derived from zone and event data, using diatoms, radiolarians, nannofossils, and foraminifers. The 14 levels are shown below:

1. Younger than 0.42 Ma from diatoms in Sample 181-1121B-1H-1, 36 cm;
2. Estimate of 0.65–1.8 Ma from diatoms in Sample 181-1121B-1H-1, 36–90 cm;
3. Estimate of 2.2–3.6 Ma from diatoms in Sample 181-1121B-1H-1, 100–102 cm;
4. Estimate of 3.26–3.6 Ma from diatoms in Sample 181-1121B-1H-1, 102–103 cm;
5. A Paleocene age, >55 Ma, using benthic foraminifers in Sample 181-1121B-3H-CC at 28.83 mbsf;
6. Radiolarian Zone RP5, 58–61 Ma, in Sample 181-1121B-6X-CC to 15X-CC; 37.01–122.33 mbsf;
7. Diatom Zone *Hemiaulus incurvus,* 58 Ma, in Samples 181-1121B-6X-CC through 12X-CC; 37.01–94.31 mbsf;
8. Radiolarian Zone RP4, 61–63 Ma, in Samples 181-1121B-15X-CC and 17X-CC; 122.04–134.47 mbsf;
9. FO of *B. tetradica,* radiolarian, 61 Ma, base of Zone RP5, in Sample 181-1121B-15X-CC; 122.04–122.33 mbsf;
10. Lower half of nannofossil Zone NP8, >56.2 Ma, in Sample 181-1121B-6X-CC; 37.01–37.28 mbsf;
11. Base of nannofossil Zone NP6, 58.4 Ma, in Sample 181-1121B-10X-CC; 76.98–77.21 mbsf;
12. Boundary between nannofossil Zones NP4 and NP5, 59.8 Ma, below Sample 181-1121B-14X-CC; 110.26 mbsf;

F18. Correlation of magnetic polarity zonations with Geomagnetic Polarity Time Scale, p. 44.

13. Upper part of nannofossil Zone NP4, ~60 Ma, in Samples 181-1121B-15X-CC through 17X-CC; 122.33–134.47 mbsf; and
14. A Paleocene age, >55 Ma, using benthic foraminifers in Samples 181-1121B-15X-CC through 17X-CC; 122.33–134.47 mbsf.

Dating of this site down to 32 mbsf is problematic (Fig. **F19**). Pliocene and Pleistocene ages are indicated in only the uppermost meter. The sequence comprises three major divisions with boundaries at 19 and 32 mbsf. Below 32 mbsf, the sediment is undoubtedly Paleocene and accumulated rapidly at 100 m/m.y. The uppermost section down to 19 mbsf is most probably Neogene and represents a residual sandy to silty product of winnowing that accumulated at <1 m/m.y. The age of the intervening section down to 32 mbsf is equivocal as it contains Paleocene radiolarians, which could be reworked (see **"Biostratigraphy,"** p. 8). This section could thus have an age anywhere from Paleocene to Miocene. It is lithologically dissimilar to the undoubted Paleocene material (except for the presence of chert) (see **"Lithostratigraphy,"** p. 3). More detail on sedimentation rate in the Paleocene is afforded by the five magnetochron boundaries, which suggest two periods of fast sedimentation with a reduction in rate to 4 m/m.y. between 81 and 93 mbsf (see **"Paleomagnetism,"** p. 15).

INORGANIC GEOCHEMISTRY

Interstitial Waters

Twelve interstitial-water samples were collected from Hole 1121B at depths ranging from 5.95 to 132.90 mbsf (Table **T6**, also in **ASCII format**). Sampling frequency is one per 10 m, with the exception of an ~30-m-long interval between 91.90 and 120.80 mbsf, which could not be sampled because of poor core recovery (Fig. **F20**).

Salinity, Chloride, and pH

Salinities of the interstitial-water samples are almost constant (34.5) throughout the hole, except for one value (34.0) at 120.80 mbsf. Chloride (Cl^-) concentrations increase from the subseafloor value of 554 mM at 5.95 mbsf to a maximum value of 565 mM at 15.40 mbsf. From 15.40 mbsf to 91.90 mbsf, chloride concentration remains relatively uniform, between 561 and 564 mM. The lowermost two samples collected in this hole show a relatively sharp decrease in chloride. Interstitial water pH values vary in a relatively narrow range between 7.55 and 7.64 (excluding two data points at 74.10 and 83.80 mbsf). These two values are probably erroneous and caused by instrumental error.

Alkalinity, Sulfate, Phosphate, Ammonium, and Dissolved Silica

Interstitial-water alkalinity remains at a near-seawater value, with a relatively narrow range between 2.70 and 3.17 mM throughout the hole. Even the most reducing interstitial water at Site 1121 is only slightly anoxic. Alkalinity in truly reducing sediments can reach levels that are tenfold higher than the highest concentration found at Site 1121, such as those sampled at Site 1119 (see **"Inorganic Geochemistry,"** p. 21, in the "Site 1119" chapter).

F19. Age-depth curve, **p. 45.**
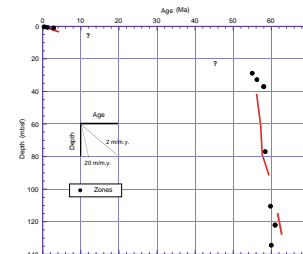
T6. Composition of interstitial waters, **p. 60.**

F20. Depth profiles of interstitial water constituents, **p. 46.**
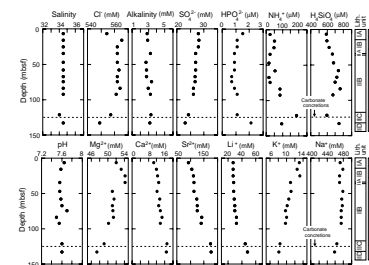
Sulfate (SO_4^{2-}) concentrations decrease gradually with depth from the seafloor to 91.90 mbsf. Microbial degradation of organic matter consumes sulfate, producing alkalinity that generates concave-downward and concave-upward profiles for sulfate and alkalinity, respectively. However, an alkalinity increase is not evident with depth at this site, indicating that some chemical reactions have masked the alkalinity increase caused by sulfate reduction. One possible reaction is the silicate reconstitution process, which decreases the alkalinity (Gieskes, 1974).

Phosphate (HPO_4^{2-}) concentrations show a slightly decreasing trend from a subseafloor value of 1.5 µM at 5.95 mbsf to a minimum value of 0.7 µM at 74.10 mbsf. Below this depth, phosphate concentration increases downhole to a maximum value of 2.1 µM at 132.90 mbsf.

Ammonium (NH_4^+) concentrations are relatively low, less than ~50 µM in the upper and middle parts of the hole (<74.10 mbsf). In the lower part of the hole, a generally increasing trend can be seen, probably because of organic matter decomposition corresponding to the slight decrease of sulfate concentration.

Dissolved silica (H_4SiO_4) concentrations increase gradually from a subseafloor value of 588 µM at 5.95 mbsf to a local maximum value of 738 µM at 57.90 mbsf, as a result of pore-fluid migration and/or diffusion driven by the concentration difference between seawater and sediments. The values of samples below 96.10 mbsf are more variable, ranging from 599 to 757 µM. A relatively high concentration zone with respect to dissolved silica corresponds to lithostratigraphic Subunit IIB, which consists of diatom and nannofossil ooze, suggesting the dissolution of siliceous tests in the sediments (see "Lithostratigraphy," p. 3). Dissolved silica concentration at 120.80 mbsf shows a relatively small value of 599 µM. This sample is taken from lithostratigraphic Subunit IIC, which consists of thin chert layers and carbonate concretions in nannofossil ooze. The decrease in dissolved silica concentration may be attributed to chert formation. Sharp decreases in dissolved silica have been recorded in association with chert horizons at other DSDP and ODP sites (Site 315, Gieskes and Lawrence, 1981; Site 495, Harrison et al., 1982).

Calcium, Magnesium, and Strontium

Calcium (Ca^{2+}) concentration shows a near-seawater value in the shallowest sample (10.6 mM at 5.95 mbsf) and increases gradually downhole to a maximum value of 16.9 mM at 120.80 mbsf.

Magnesium (Mg^{2+}) also has a near-seawater value in the shallowest sample (52.0 mM at 5.95 mbsf). There is a relatively rapid increase in the magnesium concentration in the upper part of the hole, to a maximum value of 54.1 mM at 34.10 mbsf. A relatively large shift in magnesium concentration can be seen in the interval between samples at 34.10 and 46.70 mbsf. This shift can be related to the boundary between lithostratigraphic Units I and II (34.0 mbsf), although the exact lithologic boundary is located above both of those samples. Between 46.70 and 83.80 mbsf, magnesium remains almost constant at ~51.1 mM. In the bottom part of the hole (>83.80 mbsf), magnesium concentrations decrease to a minimum value of 47.3 mM at 132.90 mbsf. The interval of magnesium decrease spans from lithostratigraphic Subunit IIB (nannofossil and diatom ooze) through Subunit IIC (chert breccia-bearing nannofossil ooze) to Subunit IID (nannofossil-bearing

clay). According to the core descriptions (see "Lithostratigraphy," p. 3), the contact between lithostratigraphic Subunits IIC and IID probably coincides with the interval used for interstitial-water sampling (interval 181-1121B-17X-2, 140–150 cm).

An unusual increase in the magnesium concentration occurs in the upper part of the hole, shallower than 34.10 mbsf. At most DSDP and ODP sites, decreasing magnesium concentrations with depth have been reported, and magnesium transport from the surface downhole is in thought to be controlled primarily by alteration reactions involving volcanic or igneous minerals (Gieskes and Lawrence, 1981). However, the increase in magnesium at Site 1121 suggests dominant ion-exchange of clay minerals and silicate reconstitution.

Strontium (Sr^{2+}) concentration generally tracks the profile of calcium concentration, showing a steady increase with depth. Strontium to calcium ratios (Sr^{2+}/Ca^{2+}) remain in a relatively narrow range between 8.7×10^{-3} and 10.3×10^{-3} mol/mol throughout the hole, although an increasing trend with depth suggests a limited effect from carbonate recrystallization.

Potassium, Lithium, and Sodium

The potassium (K^+) concentration steadily decreases throughout the hole to a minimum value of 8.1 mM at 132.90 mbsf. Potassium normally decreases with increasing burial depth at deep-sea sites. Possible sinks for potassium are authigenic K-feldspar associated with the opal transformation process (Kastner and Gieskes, 1976), illite-smectite formation (Perry and Hower, 1970), or K^+ uptake in the alteration of volcaniclastic sediment and basalt (Gieskes and Lawrence, 1981).

Concentrations of lithium (Li^+) increase slightly with depth to 91.90 mbsf. Below this depth, concentrations rapidly increase to 48 µM by 132.90 mbsf. Sodium (Na^+) concentrations do not change downcore from the subseafloor to 91.90 mbsf. Na^+ values subsequently decrease to a minimum of 458 mM at 132.90 mbsf.

Summary of Interstitial-Water Results

The profiles of interstitial-water constituents at Site 1121 show local fluctuations, suggesting dominant lithologic control rather than a simple diffusion process of diagenetic fluids. The primary chemical reactions are silica diagenesis, dissolution of carbonate, and, possibly, ion-exchange reactions of clay minerals. In particular, relatively high concentrations of dissolved silica in the interval between ~35 and 120 mbsf are related to the dissolution of biosiliceous sediments. In the lower part of the hole, relatively large shifts in concentration-depth profiles of some interstitial-water constituents (Cl^-, Mg^{2+}, HPO_4^{2-}, and MH_4^+) occur. A local decrease in dissolved silica concentration at ~120 mbsf can be related to chert formation in lithostratigraphic Subunit IIC. Low-porosity chert layers and calcium carbonate concretions may act as diffusion barriers for interstitial-water constituents.

ORGANIC GEOCHEMISTRY

Volatile Hydrocarbons

As part of the shipboard safety and pollution-prevention monitoring program, hydrocarbon gases were analyzed in each core of Hole 1121B by the headspace technique. Methane and higher hydrocarbons could only be recognized in trace concentrations (<10 ppm). These low methane concentrations indicate low bacterial activity in the sediments, probably because of organic matter limitation. This result is corroborated by almost constant sulfate concentrations in pore waters throughout the hole (see "Inorganic Geochemistry," p. 19).

Carbonate, Organic Carbon, and Organic Carbon/Nitrogen Values

The abundance of total, inorganic, and organic carbon and of calcium carbonate in sediments from Holes 1121A and 1121B is summarized in Table T7 (also in ASCII format). Random sampling of all lithologies was performed for carbonate analysis. Organic carbon was measured at a resolution of one sample per core.

Carbonate contents are highly variable throughout the section and lie in the range of 0.38 to 52.1 wt% (Fig. F21). The carbonate contents reflect varying biological productivity, and postdepositional carbonate dissolution in relation to the inferred paleowater depth and position of the lysocline.

Low organic-carbon contents (<0.36%) were found from eight measured samples. It suggests that the respiration of most of the organic matter occurred during sedimentation and early diagenesis caused by oxic water column conditions.

Ratios of organic carbon/nitrogen was calculated for Site 1121 samples using TOC and total nitrogen concentrations to help identify the origin of the organic matter. The ratios vary from 4.3 to 16.3 (Table T7). Because of (1) the small number of analyses, (2) low organic carbon and low total nitrogen contents, and (3) an obviously strong degradation of the organic matter, a clear indication of the organic matter source is not possible.

PHYSICAL PROPERTIES

Index Properties

Index properties measurements were made at a resolution of one sample every two sections in the cores from Hole 1121B. Index properties were determined by a gravimetric method (see "Physical Properties," p. 24, in the "Explanatory Notes" chapter). Values of measured index properties (void ratio, porosity, water content, bulk density, and grain density) are presented in Table T8 (also in ASCII format). Relatively low density (wet-bulk density <1.4 g/cm^3) and fairly homogeneous sediments occurred between 16 and 92 mbsf (Fig. F22). The porosity is generally higher than 70% except in the lowest part of the core (below 120 mbsf), where sediments are more compacted. Sediments recovered from this site are characterized by generally lower bulk densities and higher porosities than the previous two sites (Sites 1119 and 1120).

T7. Organic chemistry data, p. 61.

F21. Carbonate contents in sediments, p. 47.
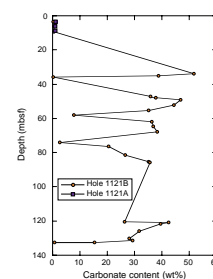
T8. List of index properties measurements, p. 62.

F22. Index properties measurements, p. 48.
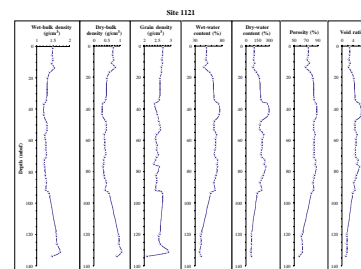
Multisensor Track Measurements

The shipboard physical properties program at Site 1121 included nondestructive measurements of bulk density, magnetic susceptibility, and natural gamma-ray activity on whole sections of all cores using the multisensor track (Fig. F23). Magnetic susceptibility was measured at 4-cm intervals and at high sensitivity (4-s measurement time) in all Site 1121 holes. Magnetic susceptibility is generally low but has higher values in the upper part of the core (<16 mbsf). Natural gamma-ray activity was measured with a 15-s count every 14 cm in Holes 1121A and 1121B. There is little variation downcore except in the upper part of the core (<16 mbsf) where high-amplitude fluctuations correlate well with the magnetic susceptibility data. High values of natural gamma radiation give an indication that clays are relatively abundant in the upper sections of the core. High-amplitude fluctuations in this portion of the core reflect interlayered sand/silt layers with clay-rich layers. Gamma-ray attenuation porosity evaluator (GRAPE) bulk density measurements were made at 4-cm intervals at all Site 1121 holes. High-amplitude fluctuations are observed in the GRAPE density over the upper part of the core. Below 20 mbsf, the sediment became less dense with little variation downcore to 94 mbsf. The GRAPE density in Hole 1121B increases in the bottom part of the core (120–134 mbsf). A comparison of GRAPE density with the wet-bulk density determined from discrete samples shows general agreement (Fig. F24). The *P*-wave velocity measurements were made at 4-cm intervals in Holes 1121A and 1121B, but gave poor results.

Shear Strength

Measurements of shear strength, using a mechanical vane, were made on split cores from Hole 1121B. Samples were generally taken in clay-rich layers showing the least disturbance by the coring process; they were chosen by visual inspection of the cores and collected at a resolution of one per section in Hole 1121B. No measurements were taken on XCB cores. Only three APC cores had sediment layers that were suitable for the vane shear test. Values gradually increase with increasing burial depth and range from 5 to 35 kPa. Shear strengths are general higher than those measured at previous sites (Sites 1119 and 1120) (Fig. F25). An approximation of the consolidation characteristics of the sediments was made by using the classic relationship between shear strength and sedimentary overburden pressure. According to Skempton (1970), normally consolidated sediments are characterized by a ratio of shear strength to overburden pressure of between 0.2 and 0.5; overconsolidated sediments are characterized by a ratio generally greater than 0.5. At Site 1121 overconsolidation exists to a depth of about 20 mbsf as a result of a once thick, but now eroded overburden. It is likely that the overburden sediments that caused the overconsolidation in the top 20 m of the core have been removed by current erosion. No Torvane shear test was made.

Compressional-Wave Velocity

Compressional-wave velocity (*P*-wave velocity) was measured parallel to the core axis on split cores from Holes 1121B using the digital sound velocimeter system. Below 120 mbsf, sediments are more consolidated than in the upper part of the core, and the Hamilton frame velocimeter

F23. MST measurements, **p. 49.**
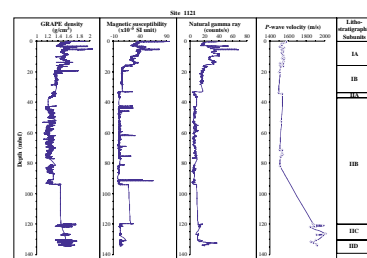
F24. Density measurements, **p. 50.**
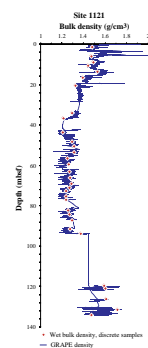
F25. Distribution of shear strength, **p. 51.**
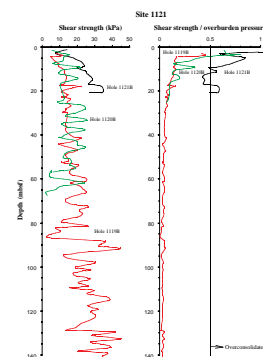
was therefore used to measure sound propagation through the sediment. These measurements gave better results than those measured by the MST. There are good correlations between the *P*-wave velocity values and the GRAPE density, magnetic susceptibility, and natural gamma radiation data in two separate zones of the core: the uppermost portion of the core (<16 mbsf), and the lowest part of the core (>120 mbsf) (Fig. F23).

Thermal Conductivity

No downhole temperature measurement with the Adara temperature tool was taken at Site 1121. Thermal conductivity, however, was measured at three intervals per core. Values obtained from thermal conductivity correlate well with those from wet-bulk density, indicating thermal conductivity depends on the density of the sediments (Fig. F26).

Discussion

Physical properties data support the lithostratigraphic zonation of the core (see "Lithostratigraphy," p. 3). Lithostratigraphic Subunit IA is characterized by high-amplitude fluctuations in the MST data. Natural gamma radiation reaches some of the highest values (67 counts/s) in the entire core in this subunit, reflecting the high clay content. Subunit IB shows very little variation in MST properties, which supports the possibility that this section of the core may consist predominantly of flow-in material. Physical properties over the interval defined as Unit II are rather uniform. The interval covered by Subunits IIA and IIB shows an average trend that is at a lower level than data values in Unit I. Deeper than 120 mbsf, there are higher values of bulk density and *P*-wave measurements that correspond to Subunits IIC and IID. The physical properties data alone cannot differentiate between these two lowermost sections.

F26. Distribution of thermal conductivity and wet-bulk density, p. 52.
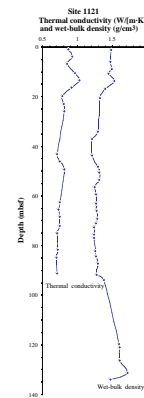
REFERENCES

Berggren, W.A., Kent, D.V., Swisher, C.C., III, and Aubry, M.-P., 1995. A revised Cenozoic geochronology and chronostratigraphy. *In* Berggren, W.A., Kent, D.V., Aubry, M.-P., and Hardenbol, J. (Eds.), *Geochronology, Time Scales and Global Stratigraphic Correlation*. Spec. Publ.—Soc. Econ. Paleontol. Mineral. (Soc. Sediment. Geol.), 54:129–212.

Bryden, H.L., and Heath, R.A., 1985. Energetic eddies at the northern edge of the Antarctic Circumpolar Current in the Southwest Pacific. *Prog. Oceanogr.,* 14:65–87.

Campbell, H.J., Andrews, P.B., Beu, A.G., Maxwell, P.A., Edwards, R.A., Laird, M.G., Hornibrook, N. de B., Mildenhall, D.C., Watters, W.A., Buckeridge, J.S., Lee, D.E., Strong, C.P., Wilson, G.J., and Hayward, B.W., 1993. Cretaceous-Cenozoic geology and biostratigraphy of the Chatham Islands, New Zealand. *Inst. Geol. Nucl. Sci. Monogr.,* 2:269.

Cande, S.C., and Kent, D.V., 1995. Revised calibration of the geomagnetic polarity timescale for the Late Cretaceous and Cenozoic. *J. Geophys. Res.,* 100:6093–6095.

Carter, L., 1989. New occurrences of manganese nodules in the South-Western Pacific Basin, east of New Zealand. *N. Z. J. Mar. Freshwater Res.,* 23:247–253.

Carter, L., Carter, R.M., McCave, I.N., and Gamble, J., 1996. Regional sediment recycling in the abyssal Southwest Pacific Ocean. *Geology,* 24:735–738.

Carter, L., and McCave, I.N., 1997. The sedimentary regime beneath the deep western boundary current inflow to the Southwest Pacific Ocean. *J. Sediment. Res.,* 67:1005–1017.

Carter, L., and Wilkin, J., in press. Abyssal circulation around New Zealand: a comparison between observations and a global circulation model. *Mar. Geol.*

Fourtanier, E., 1991. Paleocene and Eocene diatom biostratigraphy and taxonomy of eastern Indian Ocean Site 752. *In* Weissel, J., Peirce, J., Taylor, E., Alt, J., et al., *Proc. ODP, Sci. Results,* 121: College Station, TX (Ocean Drilling Program), 171–188.

Gieskes, J.M., 1974. Interstitial water studies, Leg 25. *In* Simpson, E.S.W., Schlich, R., et al., *Init. Repts. DSDP,* 25: Washington (U.S. Govt. Printing Office), 361–394.

Gieskes, J.M., and Lawrence, J.R., 1981. Alteration of volcanic matter in deep-sea sediments: evidence from the chemical composition of interstitial waters from deep sea drilling cores. *Geochim. Cosmochim. Acta,* 45:1687–1703.

Gradstein, F.M., and Berggren, W.A., 1981. Flysch-type agglutinated foraminifera and the Maestrichtian to Paleogene history of the Labrador and North seas. *Mar. Micropaleontol.,* 6:211–269.

Harrison, W.E., Hesse, R., and Gieskes, J.M., 1982. Relationship between sedimentary facies and interstitial water chemistry of slope, trench, and Cocos plate sites from the Middle America Trench transect, active margin off Guatemala, Deep Sea Drilling Project Leg 67. *In* Aubouin, J., von Huene, R., et al., *Init. Repts. DSDP,* 67: Washington (U.S. Govt. Printing Office), 603–614.

Hollis, C.J., 1997. Cretaceous-Paleocene Radiolaria of eastern Marlborough, New Zealand. *Inst. Geol. Nucl. Sci. Monogr.,* 17:1–152.

Hollis, C.J., Waghorn, D.B., Strong, C.P., and Crouch, E.M., 1997. Integrated Paleogene biostratigraphy of DSDP Site 277 (Leg 29): foraminifera, calcareous nannofossils, Radiolaria, and palynomorphs. *Inst. Geol. Nucl. Sci., Sci. Rep.,* 97/07.

Hornibrook, N. de B., Brazier, R.C., and Strong, C.P., 1989. Manual of New Zealand Permian to Pleistocene foraminiferal biostratigraphy. *Paleontol. Bull. N. Z. Geol. Surv.,* 56:1–175.

Kaiho, K., Morgans, H.E.G., and Okada, H., 1993. Faunal turnover of intermediate-water benthic foraminifera during the Paleogene in New Zealand. *Mar. Micropaleontol.,* 23:51–86.

Kastner, M., and Gieskes, J.M., 1976. Interstitial water profiles and sites of diagenetic reactions, Leg 35, DSDP, Bellingshausen Abyssal Plain. *Earth Planet. Sci. Lett.,* 33:11–20.

Kennett, J.P., 1977. Cenozoic evolution of Antarctic glaciation, the circum-Antarctic Ocean, and their impact on global paleoceanography. *J. Geophys. Res.,* 82:3843–3860.

————, 1982. *Marine Geology:* Englewood Cliffs, NJ (Prentice-Hall).

Kennett, J.P., Houtz, R.E., et al., 1975. *Init. Repts. DSDP,* 29: Washington (U.S. Govt. Printing Office).

Kennett, J.P., von der Borch, C.C., et al., 1986. *Init. Repts. DSDP,* 90: Washington (U.S. Govt. Printing Office).

Lawver, L.A., and Gahagan, L.M., 1994. Constraints on timing of extension in the Ross Sea region. *Terra Antarct.,* 1:545–552.

Martini, E., 1971. Standard Tertiary and Quaternary calcareous nannoplankton zonation. *In* Farinacci, A. (Ed.), *Proc. 2nd Int. Conf. Planktonic Microfossils Roma:* Rome (Ed. Tecnosci.), 2:739–785.

McCave, I.N., 1988. Biological pumping upwards of the coarse fraction of deep-sea sediments. *J. Sediment. Petrol.,* 58:148–158.

McCave, I.N., and Carter, L., 1997. Recent sedimentation beneath the Deep Western Boundary Current off northern New Zealand. *Deep-Sea Res.,* 44:1203–1237.

Morrow, R., Church, J., Coleman, R., Chelton, D., and White, N., 1992. Eddy momentum flux and its contribution to the Southern Ocean momentum balance. *Nature,* 357:482–484.

Orsi, A.H., Whitworth, T., III, and Nowlin, W.D., Jr., 1995. On the meridional extent and fronts of the Antarctic Circumpolar Current. *Deep-Sea Res.,* 42:641–673.

Perch-Nielsen, K., 1985. Cenozoic calcareous nannofossils. *In* Bolli, H.M., Saunders, J.B., and Perch-Nielsen, K. (Eds.), *Plankton Stratigraphy:* Cambridge (Cambridge Univ. Press), 427–554.

Perry, E., and Hower, J., 1970. Burial diagenesis in Gulf Coast pelitic sediments. *Clays Clay Miner.,* 18:165–177.

Raine, J.I., Strong, C.P., and Wilson, G.J., 1993. Biostratigraphic revision of petroleum exploration wells, Great South Basin, New Zealand. *Inst. Geol. Nucl. Sci., Sci. Rep.,* 93/32.

Roberts, A.P., Stoner, J.S., and Richter, C., 1996. Coring induced magnetic overprints and limitations of the long-core paleomagnetic measurements technique: some observations from Leg 160, eastern Mediterranean Sea. *In* Emeis, K.-C., Robertson, A.H.F., Richter, C., et al., *Proc. ODP, Init. Repts.,* 160: College Station, TX (Ocean Drilling Program), 497–505.

Roberts, A.P., and Turner, G.M., 1993. Diagenetic formation of ferrimagnetic iron sulphide minerals in rapidly deposited marine sediments, South Island, New Zealand. *Earth Planet. Sci. Lett.,* 115:257–273.

Shipboard Scientific Party, 1975. Site 276. *In* Kennett, J.P., Houtz, R.E., et al., *Init. Repts. DSDP,* 29: Washington (U.S. Govt. Printing Office), 1155–1169.

Skempton, A.W., 1970. The consolidation of clays by gravitational compaction. *Q. J. Geol. Soc. London,* 125:373–411.

Strong, C.P., Hollis, C.J., and Wilson, G.J., 1995. Foraminiferal, radiolarian, and dinoflagellate biostratigraphy of late Cretaceous to middle Eocene pelagic sediments (Muzzle Group), Mead Stream, Marlborough, New Zealand. *N. Z. J. Geol. Geophys.,* 38:171–209.

Turner, G.M., and Kamp, P.J.J., 1990. Paleomagnetic location of the Jaramillo Subchron and the Matuyama-Brunhes transition in the Castlecliffian stratotype section, Wanganui Basin, New Zealand. *Earth Planet. Sci. Lett.,* 100:42–50.

van Andel, T.H., 1975. Mesozoic/Cenozoic calcite compensation depth and the global distribution of calcareous sediments. *Earth Planet. Sci. Lett.,* 26:187–194.

Wilson, G.S., and Roberts, A.P., 1981. Deep-sea drilling interstitial water studies: implications for chemical alteration of the oceanic crust layers I and II. *In* Warme, J.E., Douglas, R.G., and Winter, E.L., (Eds.), *The Deep Sea Drilling Project: A Decade of Progress.* Spec. Publ.—Soc. Econ. Paleontol. Mineral., 32:149–167.

————, 1999. Diagenesis of magnetic mineral assemblages in multiply redeposited siliciclastic marine sediments, Wanganui Basin, New Zealand. *Geol. Soc. Spec. Publ. London,* 151:95–108.

Figure F1. Location of Site 1121 and seismic line NIWA 3034.
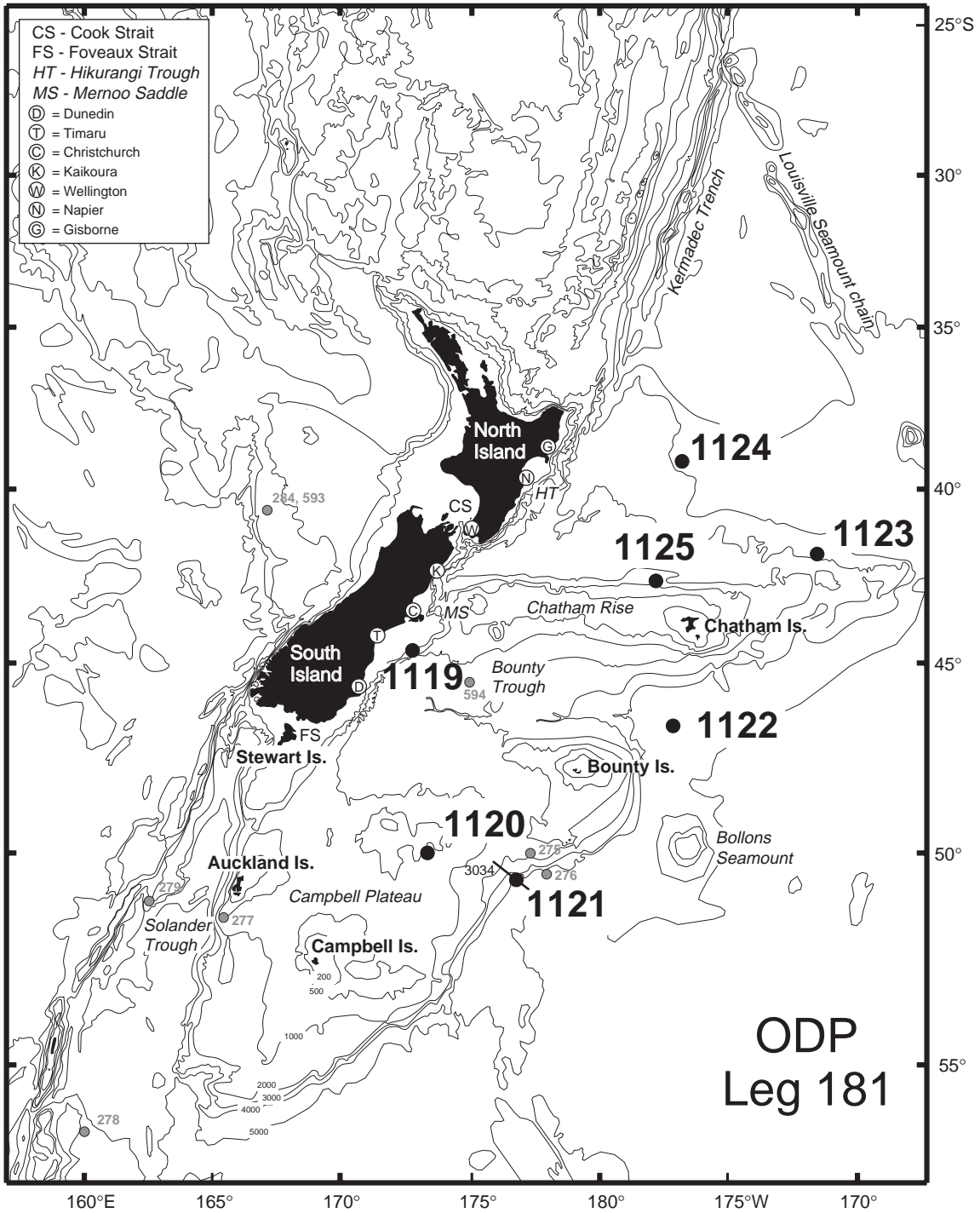
Figure F2. Part of seismic profile NIWA 3034 through Site 1121 (0315–0400 hr) with major reflectors (R1-3) delimiting seismic units A–C.

Figure F3. Summary log for Site 1121.
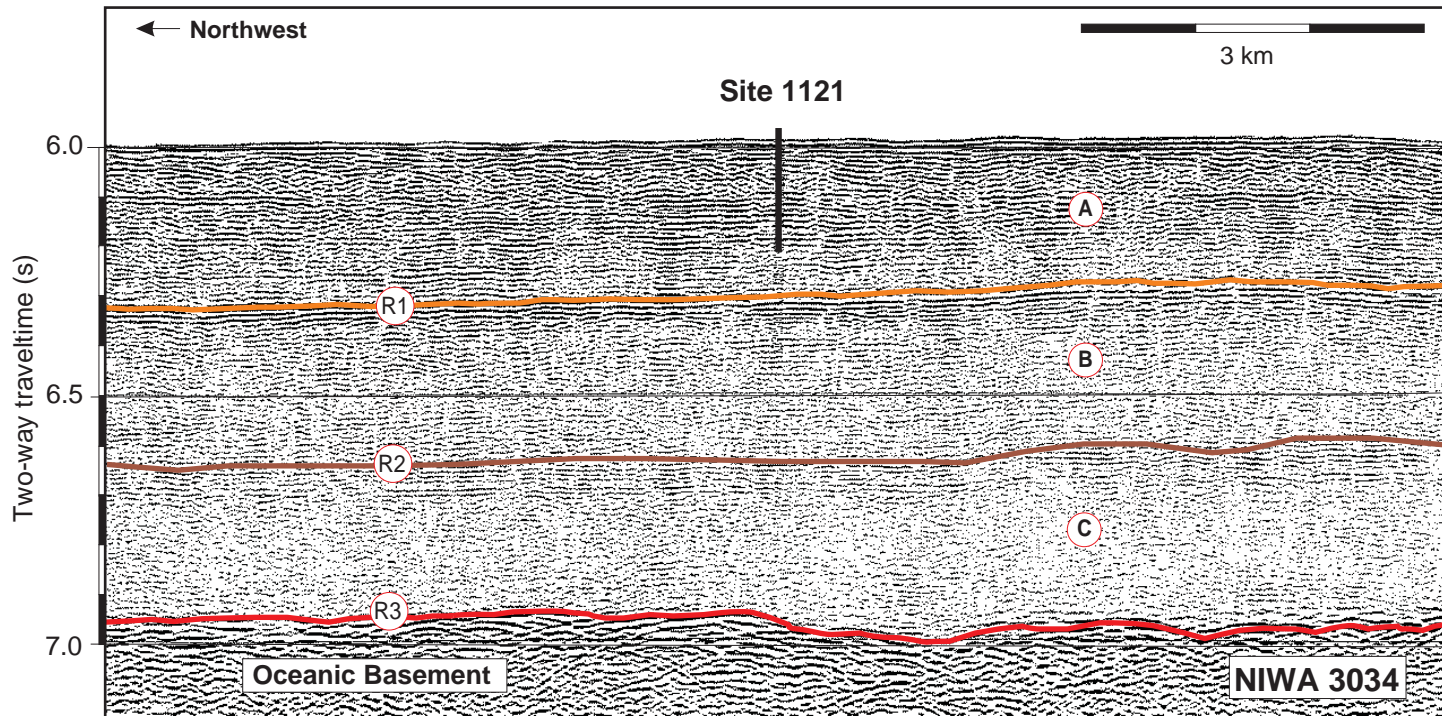
Figure F4. Bioturbation (*Thalassinoides*) of brown silty clay in Subunit IA, 6.25–6.60 mbsf (interval 181-1121B-1H-5, 25–60 cm).

Figure F5. Brownish yellow sand with a sharp bottom contact (74.5 cm) with yellow clay below in Subunit IA, 9.50–9.82 mbsf (interval 181-1121B-1H-7 through 1H-CC, 50–82 cm).

Figure F6. Ferromanganese nodules and ferromanganese sand in Subunit IA, 3.14–3.47 mbsf. The top nodule was cored through (interval 181-1121B-1H-3, 14–47 cm).

Figure F7. Two ferromanganese crusts with possible intervening zone of alteration in Subunit IA, 5.02–5.61 mbsf (interval 181-1121B-1H-4, 52–110 cm).

Figure F8. Pale yellow clay with chert nodule from Subunit IB, 16.30–16.60 mbsf (interval 181-1121B-2H-5, 80–110 cm).

Figure F9. A biostratigraphic summary chart of Site 1121 showing correlation between the four microfossil zonations and their age assignmens.

Figure F10. Age assignments, based on planktonic diatoms, for the upper 3 m of Hole 1121B.

Hole 1121B
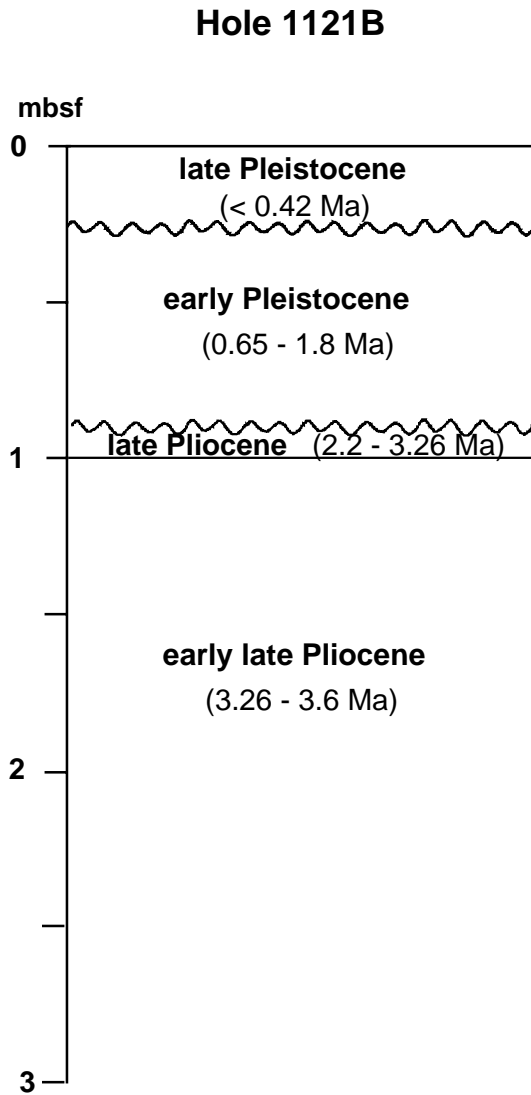
Figure F11. Tentative model of oceanic crust subsidence and CCD history at Site 1121. For details see **"Paleoenvironment,"** p. 13.
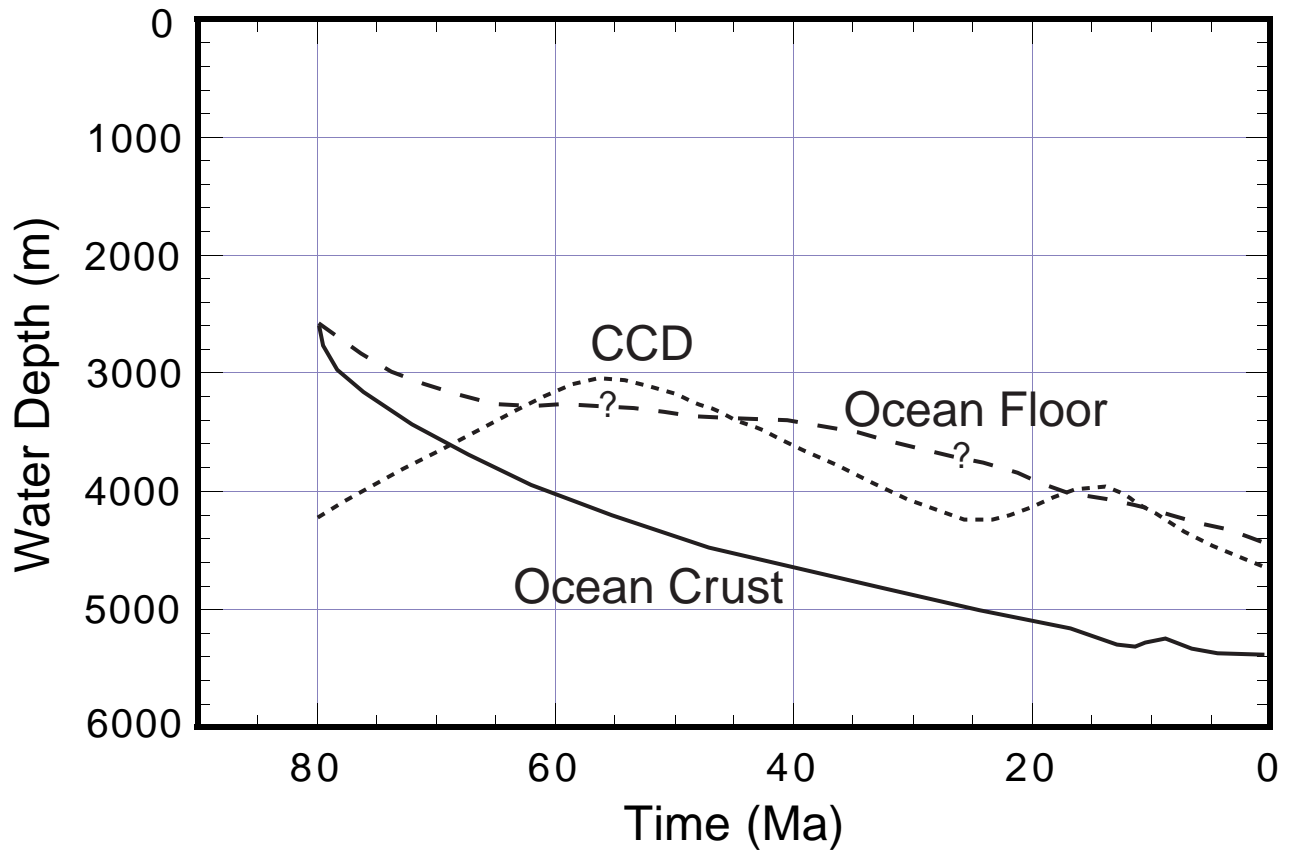
Figure F12. Relative abundance of diatom valves and of the authigenically formed zeolites, clinoptilolites, and phillipsite through Hole 1121B. B = barren, T = trace, R = rare, F = few, C = common, D = dominant.
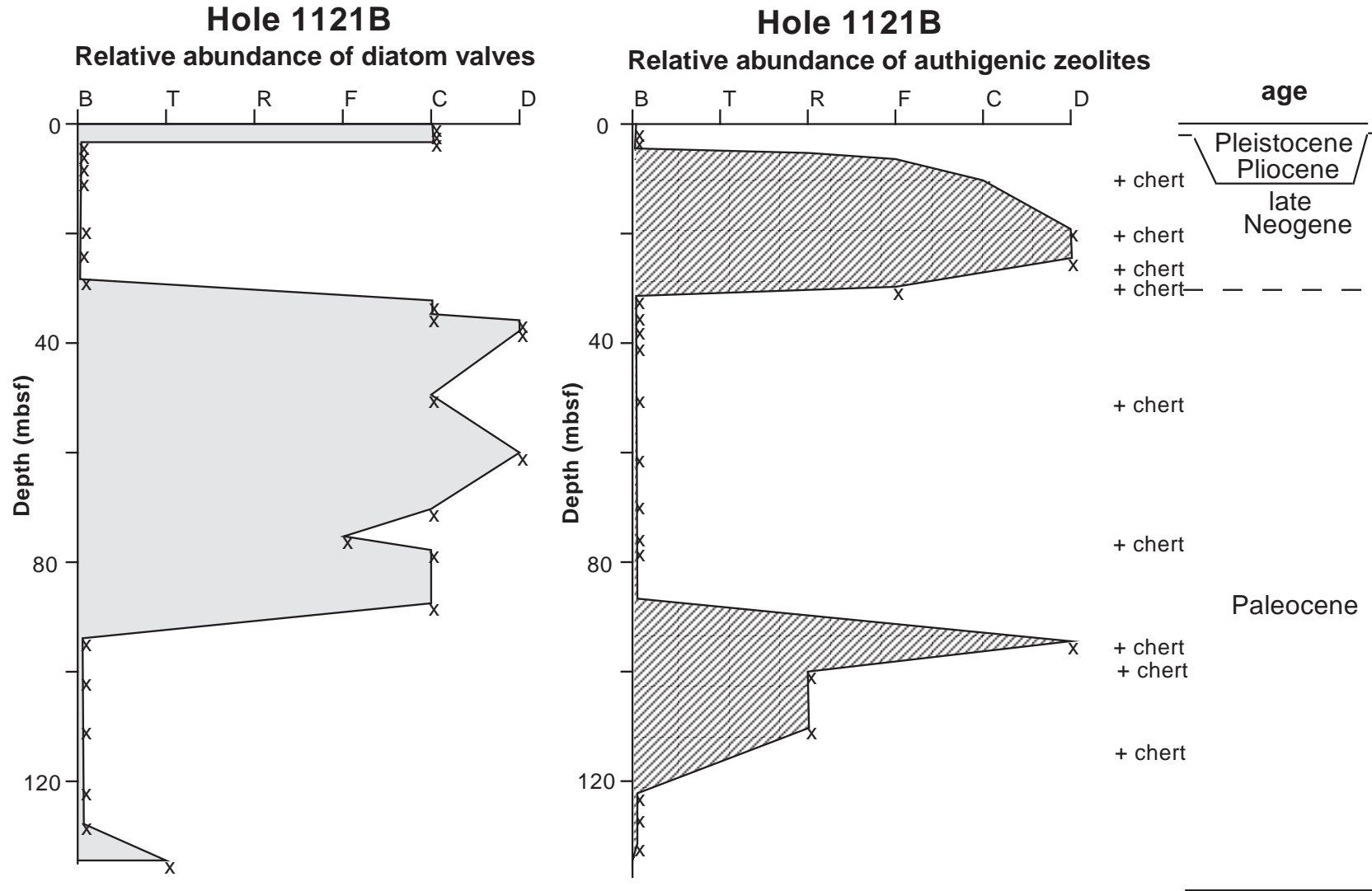
Figure F13. Whole-core magnetic susceptibility from Hole 1121B from the Bartington loop of the shipboard automated multisensor track, archive-half continuous measurements of NRM intensity and inclination before and after alternating-field demagnetization to 20 mT from the pass-though cryogenic magnetometer. Vertical and subvertical lines between 27–52 and 76–130 mbsf indicate intervals where measurements were not possible because of poor core recovery or nonrecovery. Polarity interpretation is given on the right. Black (white) shaded intervals indicate normal (reversed) polarity, and hatched shading indicates intervals where polarity could not be determined because of "flow-in," poor recovery, or nonrecovery. Interpretations of magnetochrons from correlation to the GPTS are labeled, where known (see discussion in text).
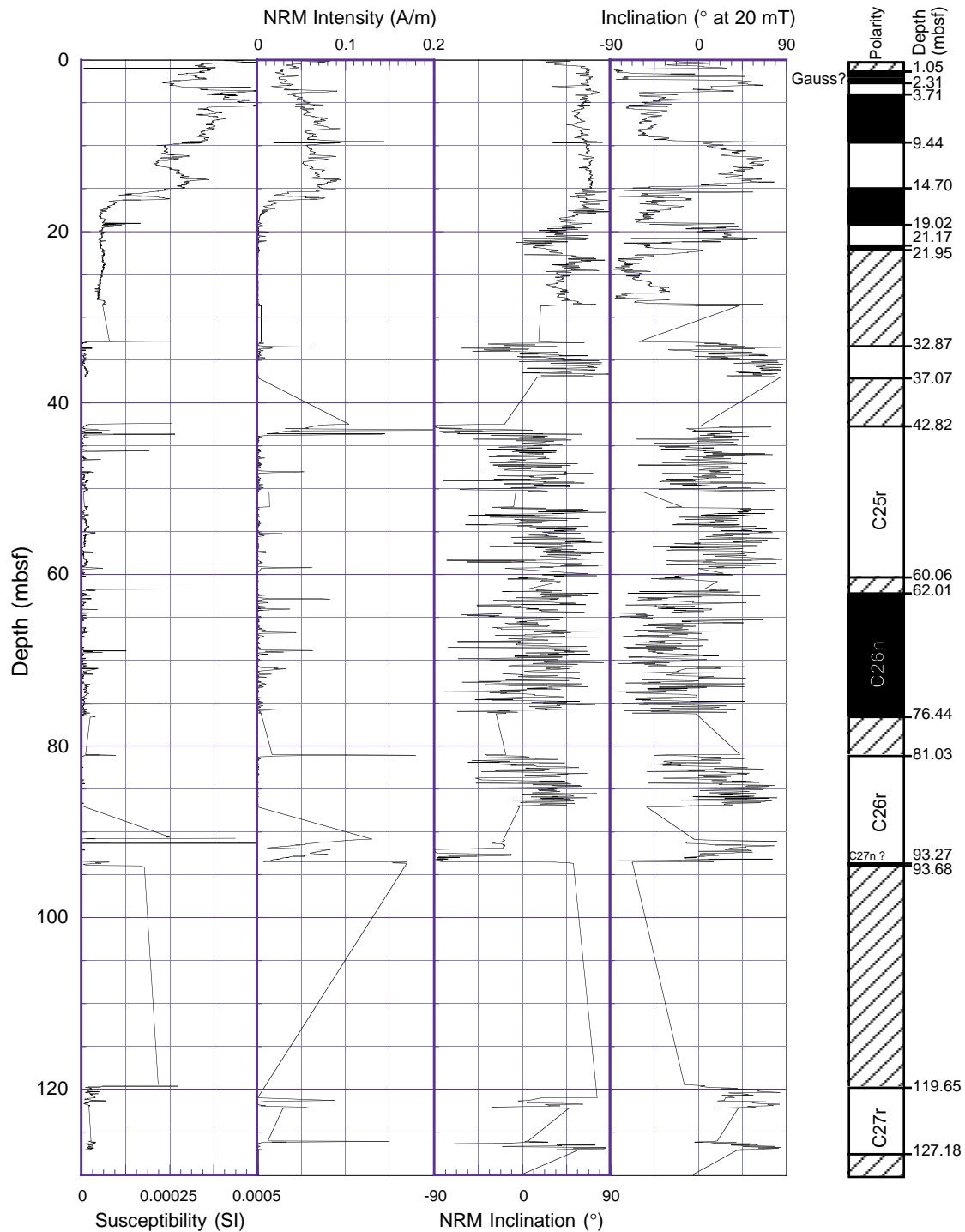
Figure F14. Whole-core magnetic susceptibility for the upper 25 mbsf of core from Hole 1121B from the Bartington loop of the shipboard automated multisensor track, archive-half continuous measurements of NRM intensity, and inclination before and after alternating-field demagnetization to 20 mT from the pass-though cryogenic magnetometer. Polarity interpretation is given on the right. Black (white) shaded intervals indicate normal (reversed) polarity, and hatched shading indicates intervals where polarity could not be determined because of "flow-in" or poor recovery. Unambiguous correlation of magnetochrons with the GPTS was not possible (see discussion in text).
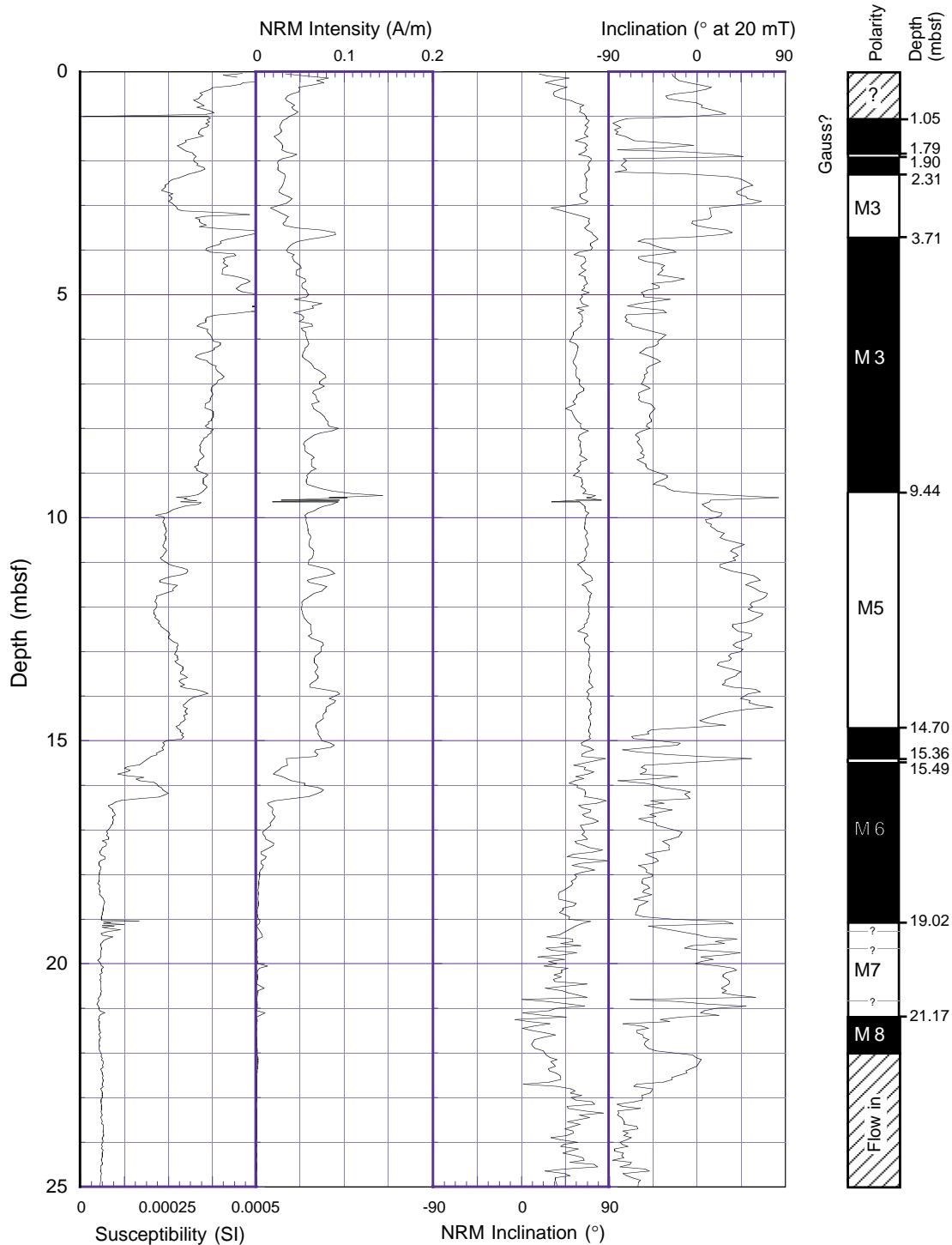
Figure F15. A–D. Vector component and equal-area diagrams of AF demagnetization behavior of representative discrete samples from Site 1121.
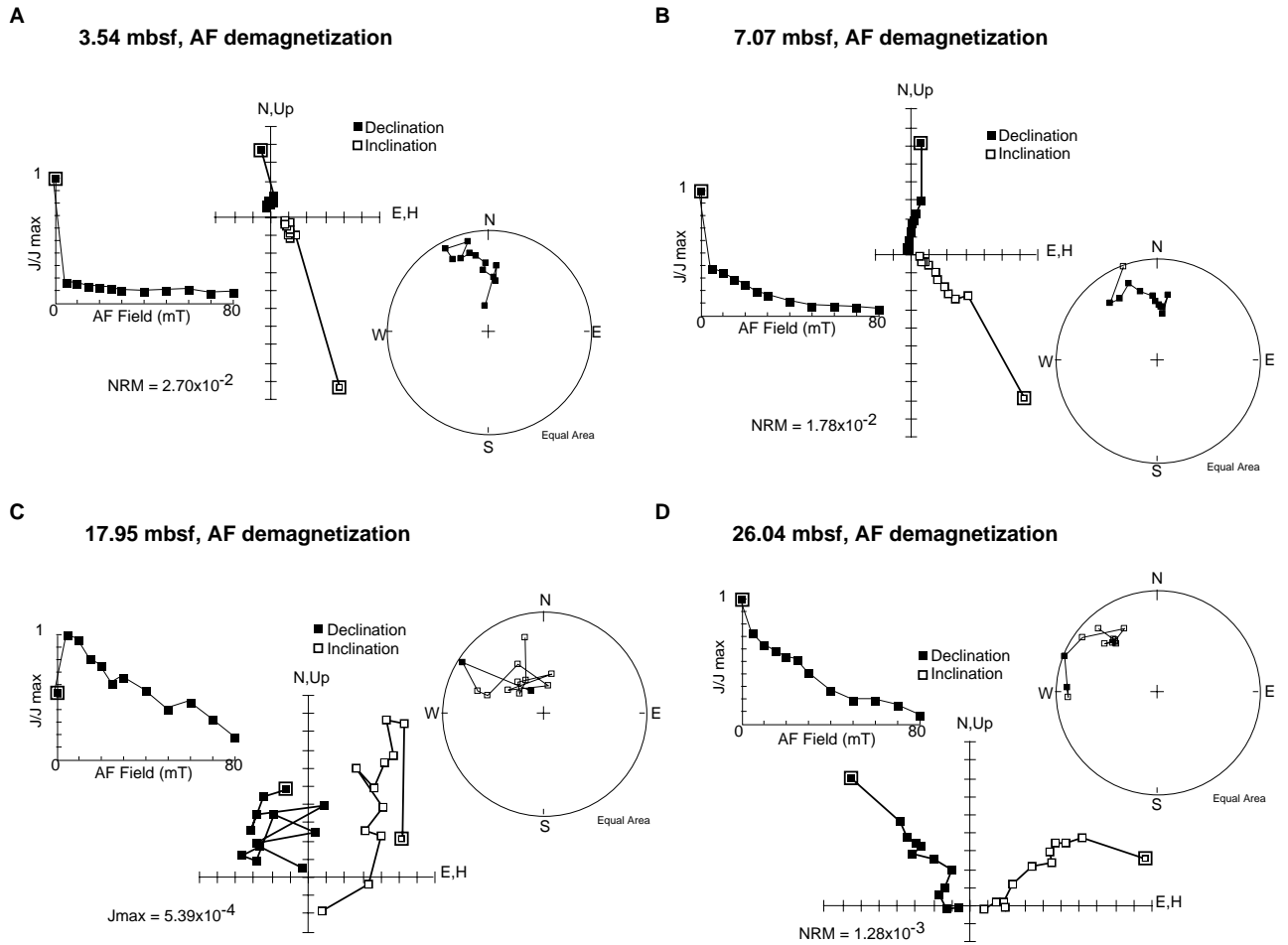
Figure F16. A. Isothermal remanent magnetization (IRM) and backfield acquisition curves for representative discrete samples from lithostratigraphic Unit I of Site 1121. Remanence does not become saturated until 200–500 mT, and B_{cr} is <50 mT for all samples. **B.** Isothermal remanent magnetization (IRM) and backfield acquisition curves for representative discrete samples from Unit II of Site 1121. Remanence does not become saturated until 500–1000 mT, and B_{cr} is between 75 and 100 mT for all samples.
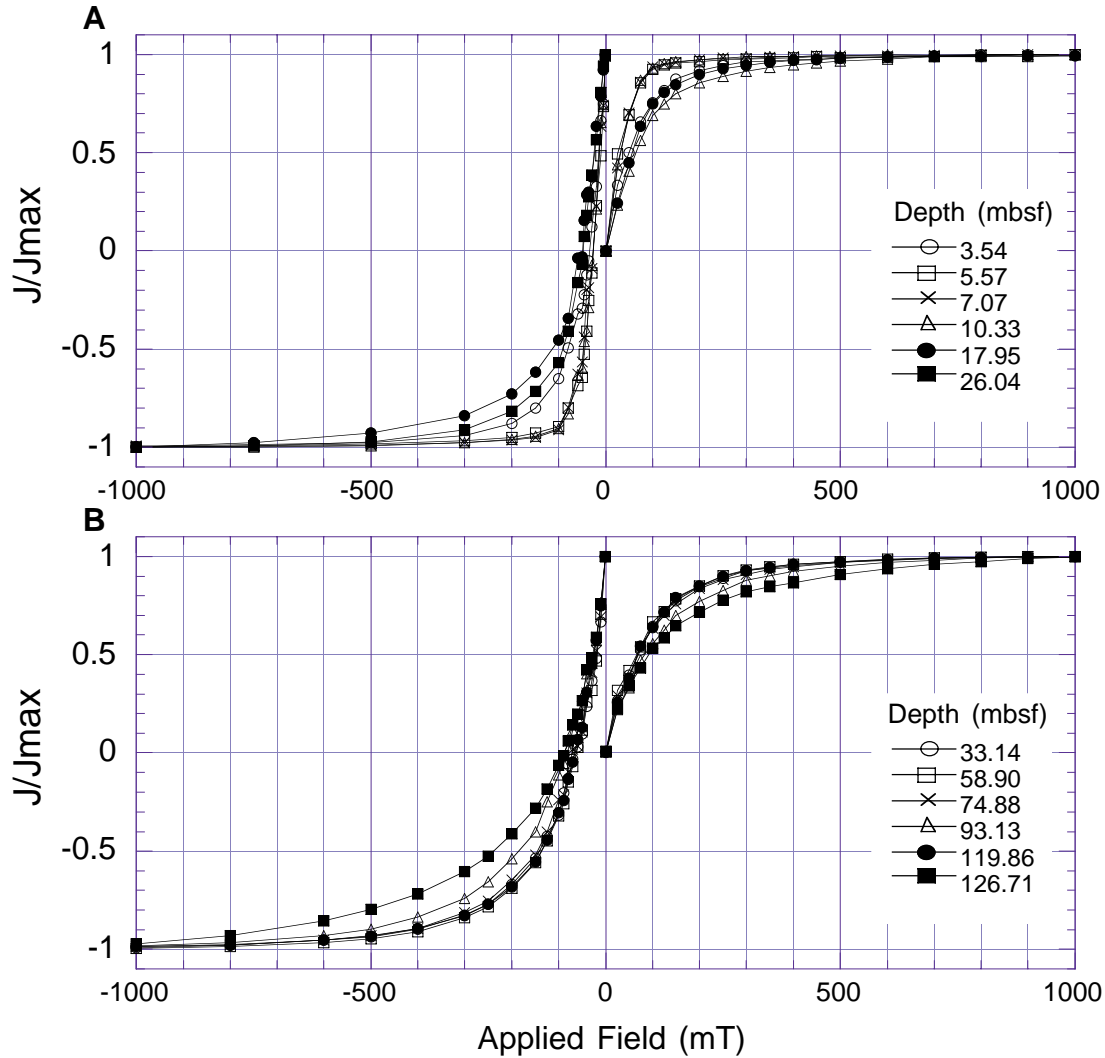
Figure F17. A–F. Plots of normalized intensity of magnetization with progressive AF and thermal demagnetization of saturation isothermal remanent magnetization (SIRM) for selected samples from Hole 1121B.
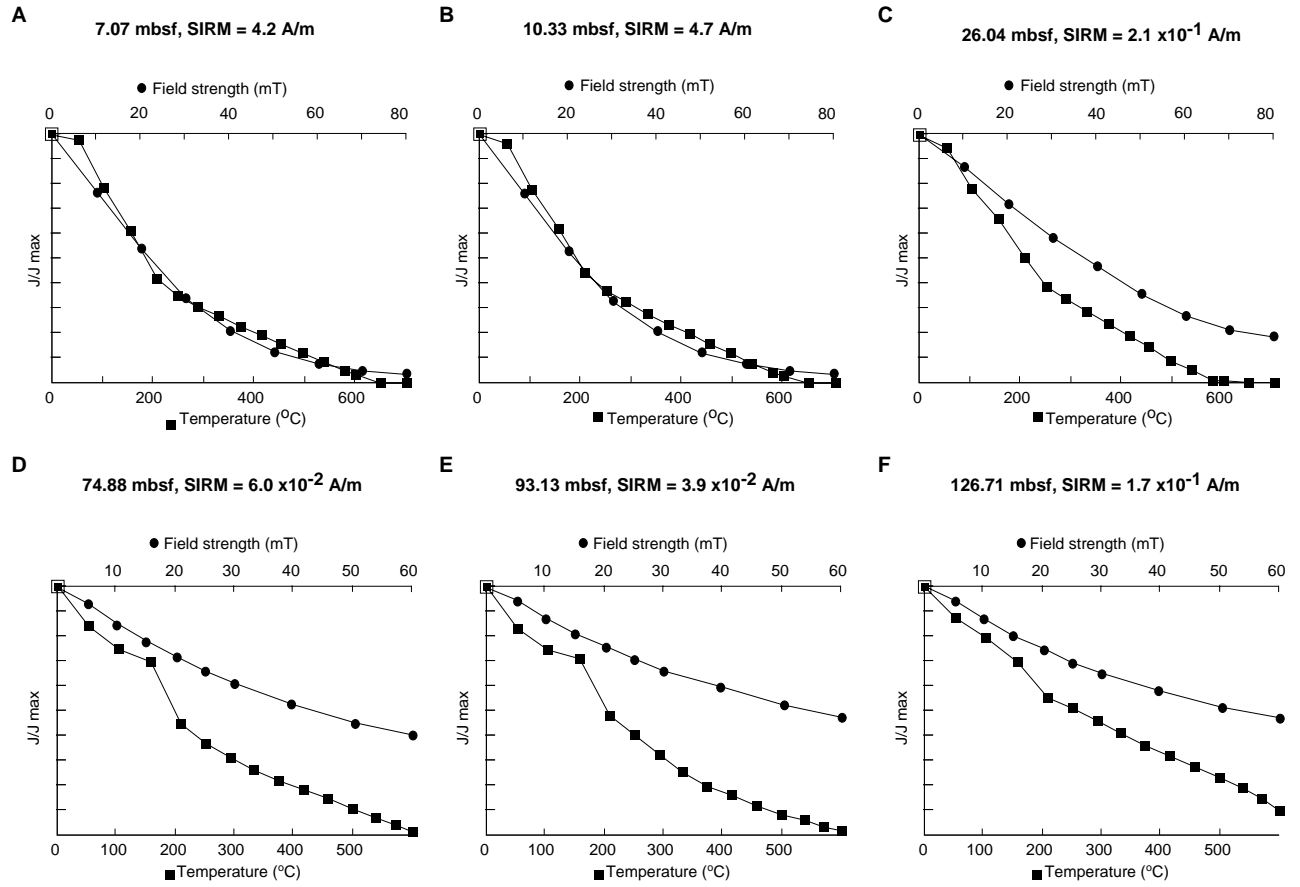
Figure F18. Correlation of Hole 1121B magnetic polarity zonations with the Geomagnetic Polarity Time Scale (GPTS) of Berggren et al. (1995) and Cande and Kent (1995). Black (white) shaded intervals indicate normal (reversed) polarity and hatched shading indicates intervals where polarity could not be determined because of "flow-in," poor recovery, or nonrecovery. Stippled and dashed lines show tie points for the correlation. Correlation is constrained by radiolarian and nannofossil zones determined for Hole 1121B (see discussion in text and "Biostratigraphy," p. 8).
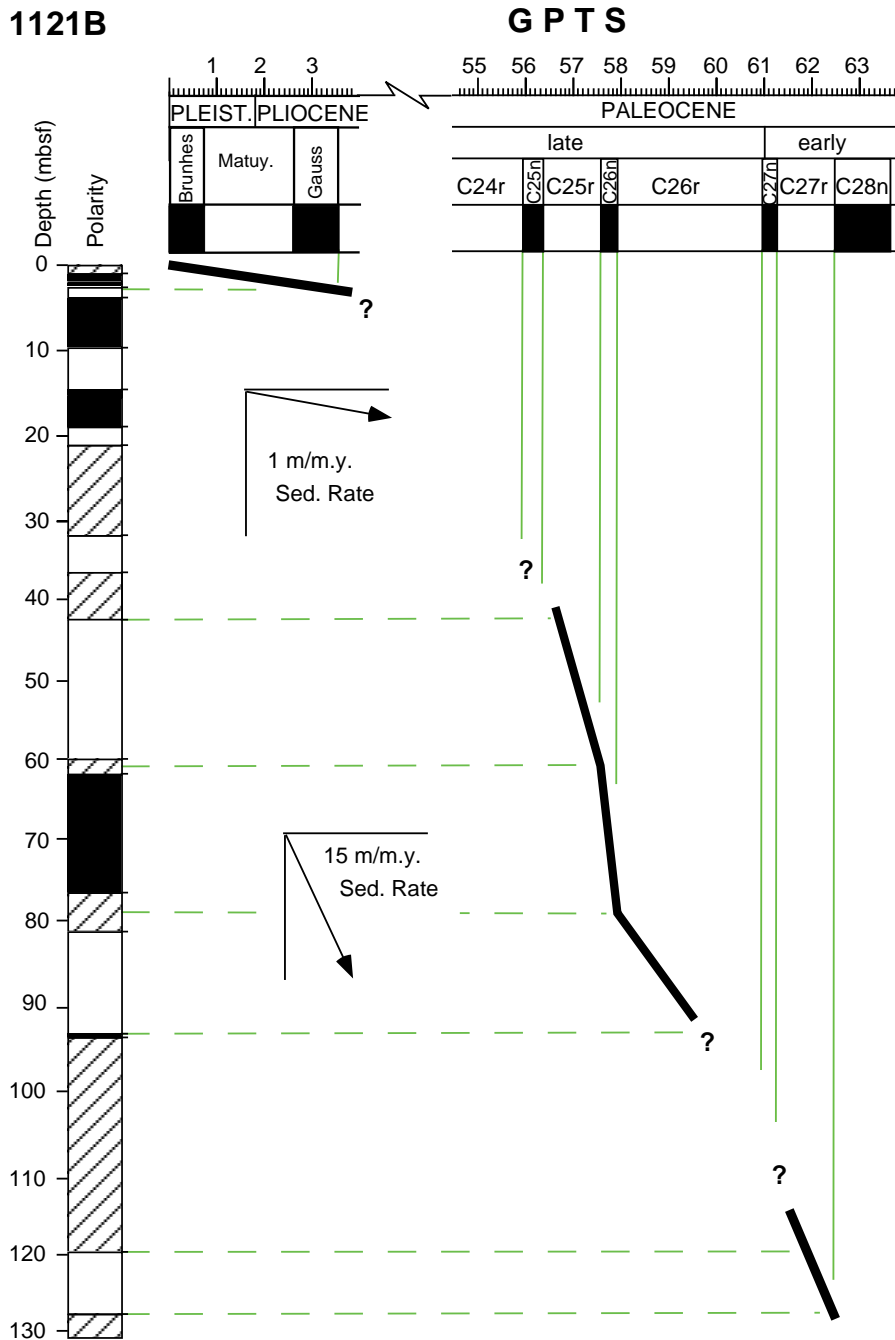
Figure F19. Age-depth curve using multiple microfossil zones and polarity chrons for Site 1121. The solid line indicates polarity correlations. The best fit line is from "Paleomagnetism," p. 15, and shows the average rate of sedimentation where correlation is possible.
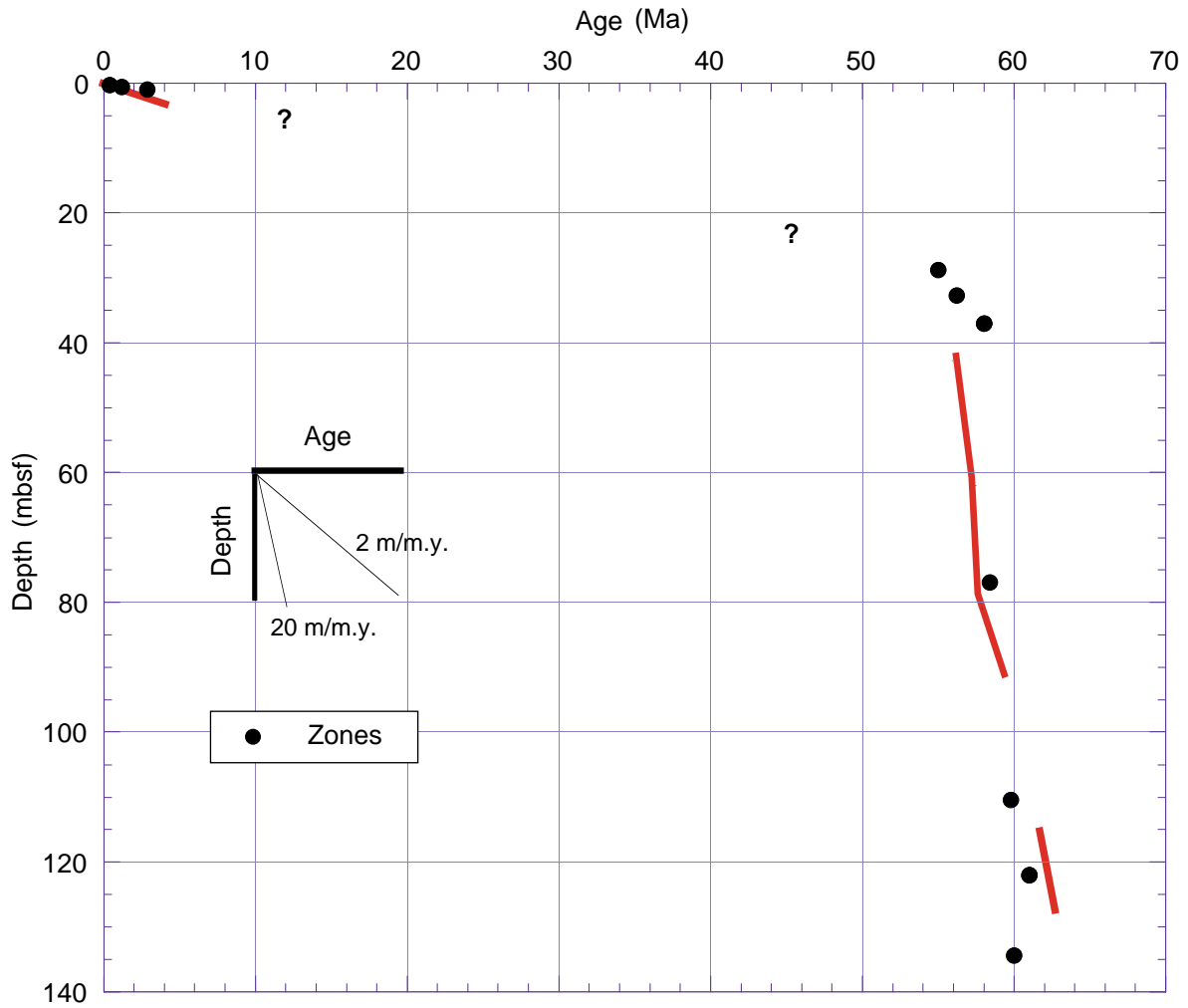
Figure F20. Depth profiles of interstitial water constituents at Site 1121.
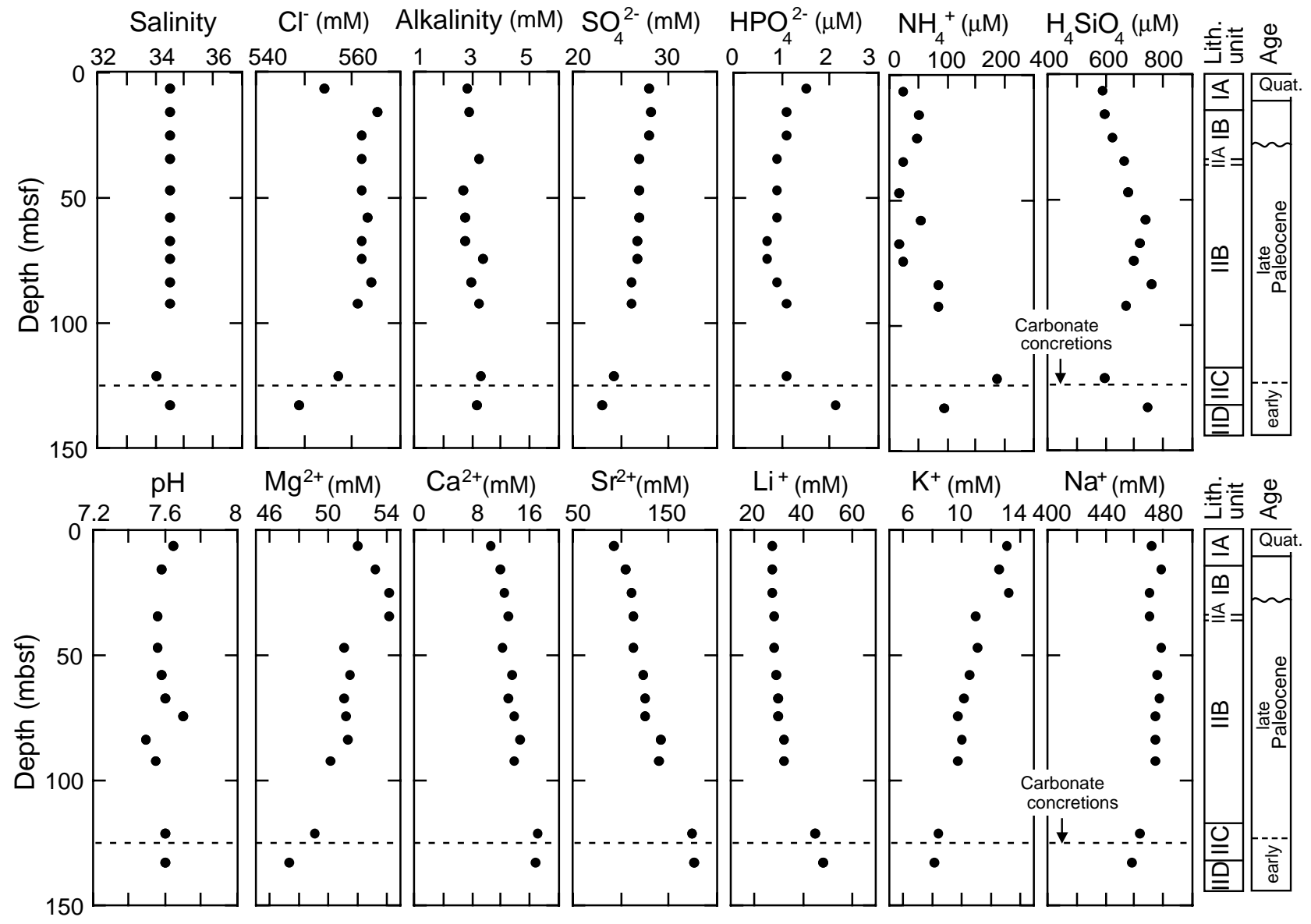
Figure F21. Carbonate contents in sediments from Holes 1121A and 1121B.
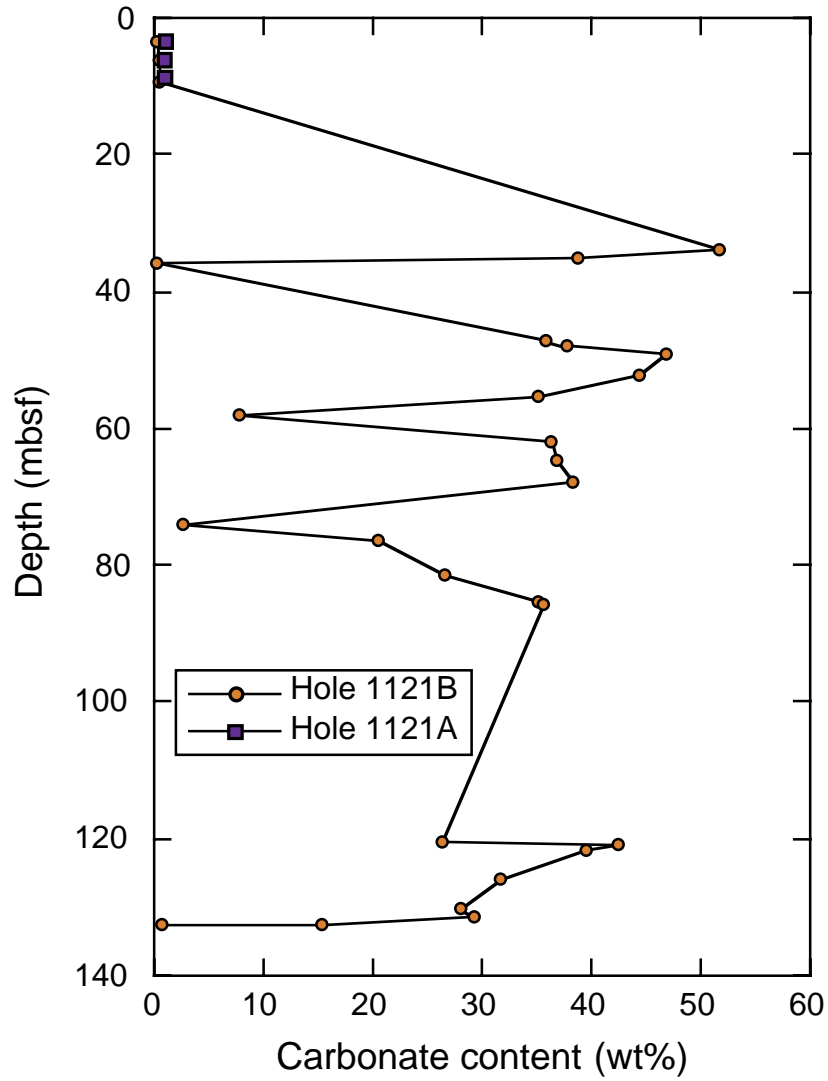
Figure F22. Index properties measurements from cores from Hole 1121B.

Figure F23. MST measurements from Hole 1121B including GRAPE density, magnetic susceptibility, and natural gamma-ray intensity. Discrete *P*-wave velocity measurements obtained from split cores.
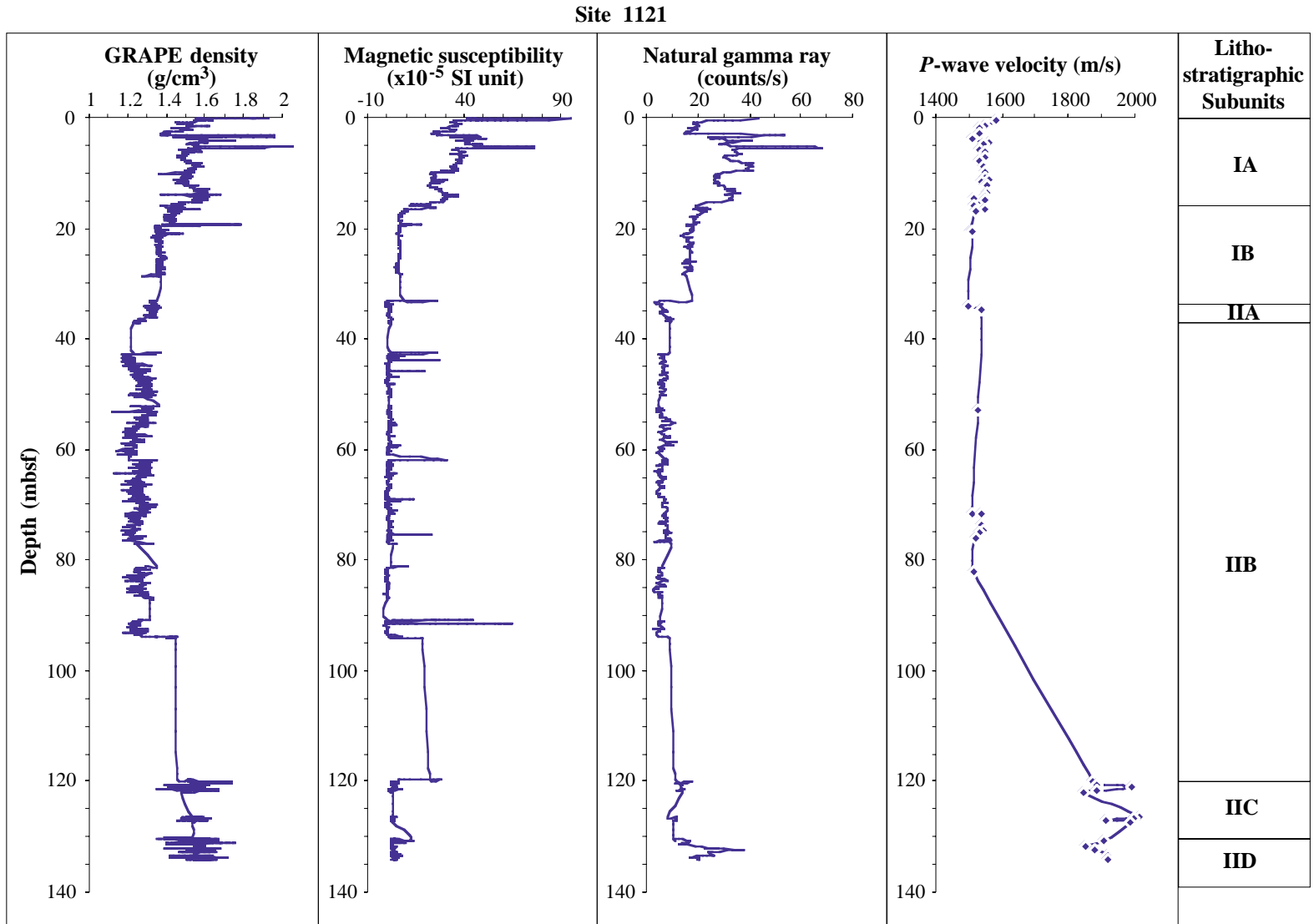
Figure F24. Density measurements using the GRAPE instrument on the MST in comparison with those from index properties. The diamond markers indicate the distribution of wet-bulk density based on index property measurement.
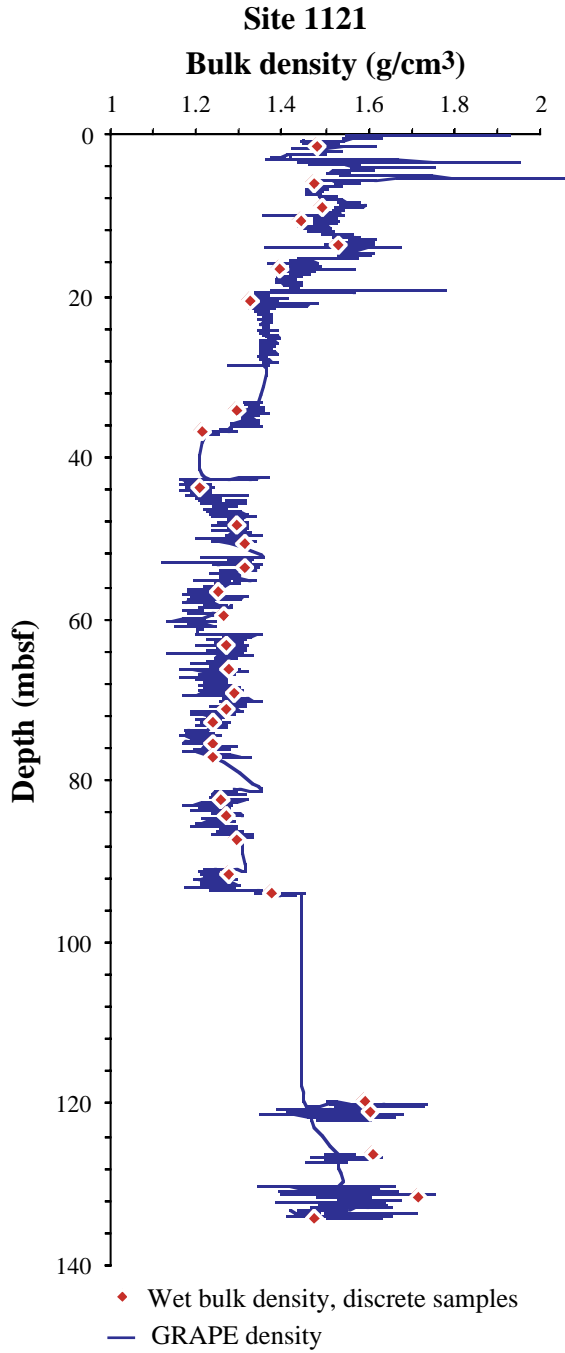
Figure F25. Distribution of shear strength in cores and the ratio of vane shear strength to overburden pressure determined from Holes 1119B, 1120B, and 1121B.

Site 1121

CHAPTER 5, SITE 1121: THE CAMPBELL "DRIFT"   **52**
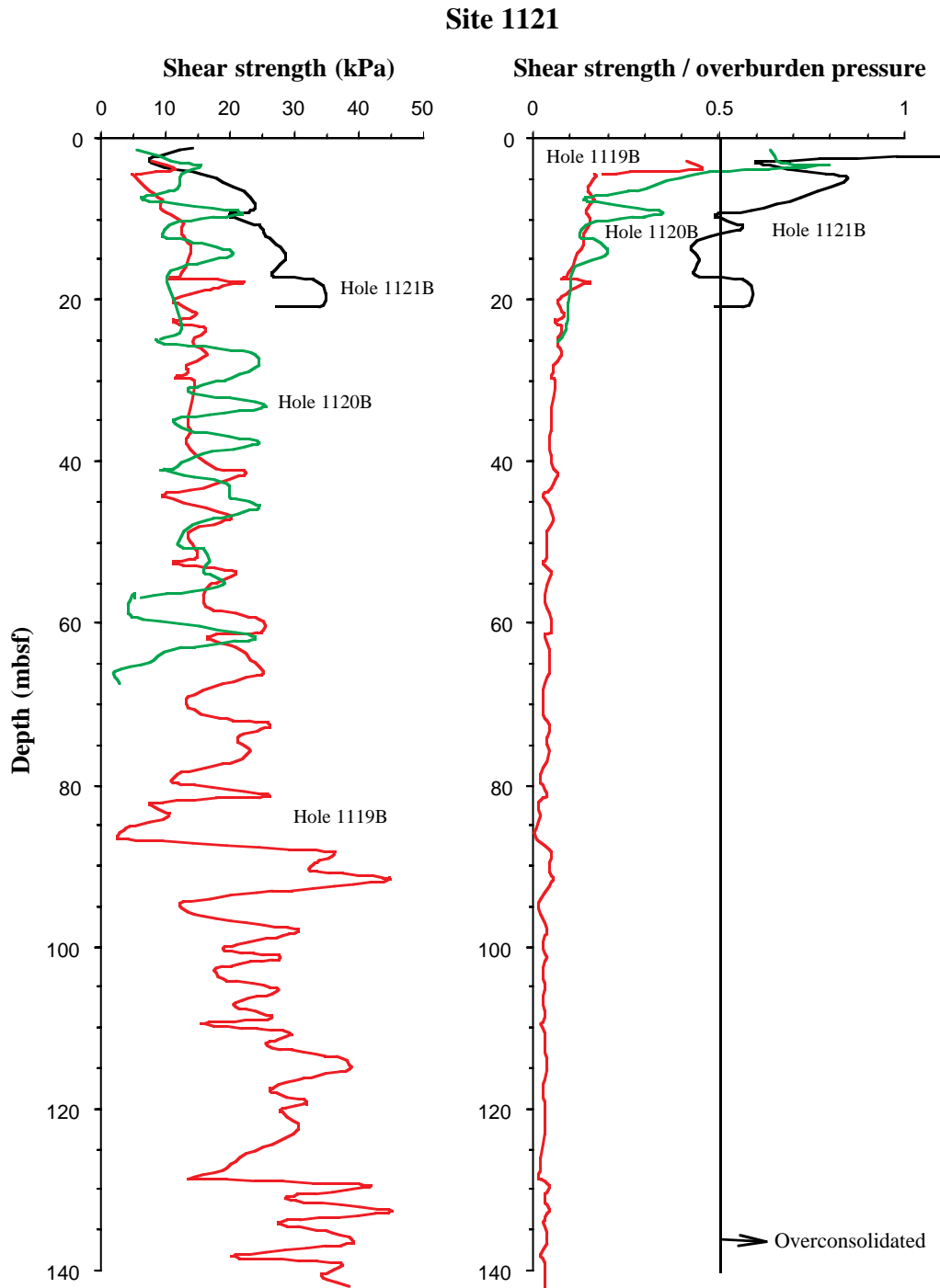
Figure F26. The distribution of thermal conductivity and wet-bulk density measured in cores from Hole 1121B.

Site 1121
Thermal conductivity (W/[m·K])
and wet-bulk density (g/cm^3)

Table T1. Site 1121 expanded coring summary. (**See table note.** Continued on next two pages.)

Core	Date (September 1998)	Time (UTC)	Core depth (mbsf)		Length (m)		Recovery (%)	Section	Length (m)		Section depth (mbsf)		Catwalk samples	Comment
			Top	Bottom	Cored	Recovered			Liner	Curated	Top	Bottom		
181-1121A-														
1H	2	420	0	8.4	8.4	8.37	99.6							
								1	1.5	1.5	0	1.5		
								2	1.5	1.5	1.5	3		
								3	1.5	1.5	3	4.5		
								4	1.5	1.5	4.5	6		
								5	1.5	1.5	6	7.5		
								6	0.6	0.6	7.5	8.1		
								CC	0.27	0.27	8.1	8.37	PAL	
									8.37	8.37				
				Totals:	8.4	8.37	99.60							
181-1121B-														
1H	2	0540	0	9.5	9.5	9.92	104.4							
								1	1.5	1.5	0	1.5		
								2	1.5	1.5	1.5	3		
								3	1.5	1.5	3	4.5		
								4	1.5	1.5	4.5	6	IW	
								5	1.5	1.5	6	7.5	HS	
								6	1.5	1.5	7.5	9		
								7	0.7	0.7	9	9.7		
								CC	0.22	0.22	9.7	9.92	PAL, PAL, PAL	
									9.92	9.92				
2H	2	0655	9.5	19	9.5	9.93	104.5							
								1	1.5	1.5	9.5	11		
								2	1.5	1.5	11	12.5		
								3	1.5	1.5	12.5	14		
								4	1.5	1.5	14	15.5	IW	
								5	1.5	1.5	15.5	17	HS	
								6	1.5	1.5	17	18.5		
								7	0.76	0.76	18.5	19.26		
								CC	0.17	0.17	19.26	19.43	PAL	
									9.93	9.93				
3H	2	0825	19	23	4	9.83	245.8							
								1	1.5	1.5	19	20.5		
								2	1.5	1.5	20.5	22		
								3	1.5	1.5	22	23.5		
								4	1.5	1.5	23.5	25	IW	
								5	1.5	1.5	25	26.5	HS	
								6	1.5	1.5	26.5	28		
								7	0.68	0.68	28	28.68		
								CC	0.15	0.15	28.68	28.83	PAL	
									9.83	9.83				
4X	2	1040	23	23.5	0.5	0.28	56							
								CC	0.28	0.28	23	23.28	PAL	

Core	Date (September 1998)	Time (UTC)	Core depth (mbsf) Top	Bottom	Length (m) Cored	Recovered	Recovery (%)	Section	Length (m) Liner	Curated	Section depth (mbsf) Top	Bottom	Catwalk samples	Comment
									0.28	0.28				
5X	2	1240	23.5	32.7	9.2	0.27	2.9							
								CC	0.27	0.27	23.5	23.77	PAL	
									0.27	0.27				
6X	2	1350	32.7	42.3	9.6	4.58	47.7							
								1	1.5	1.5	32.7	34.2	IW	
								2	1.5	1.5	34.2	35.7	HS, PAL	
								3	1.31	1.31	35.7	37.01		
								CC	0.27	0.27	37.01	37.28	PAL	
									4.58	4.58				
7X	2	1455	42.3	52	9.7	8.35	86.1							
								1	1.5	1.5	42.3	43.8		
								2	1.5	1.5	43.8	45.3		
								3	1.5	1.5	45.3	46.8	IW	
								4	1.5	1.5	46.8	48.3	HS	
								5	1.5	1.5	48.3	49.8		
								6	0.62	0.62	49.8	50.42		
								CC	0.23	0.23	50.42	50.65	PAL	
									8.35	8.35				
8X	2	1600	52	61.6	9.6	9.06	94.4							
								1	1.5	1.5	52	53.5		
								2	1.5	1.5	53.5	55		
								3	1.5	1.5	55	56.5		
								4	1.5	1.5	56.5	58	IW	
								5	1.35	1.35	58	59.4	HS	
								6	1.5	1.5	59.35	60.85		
								CC	0.21	0.21	60.85	61.06	PAL	
									9.06	9.06				
9X	2	1655	61.6	71.2	9.6	9.68	100.8							
								1	1.5	1.5	61.6	63.1		
								2	1.5	1.5	63.1	64.6		
								3	1.5	1.5	64.6	66.1		
								4	1.5	1.5	66.1	67.6	IW	
								5	1.5	1.5	67.6	69.1	HS	
								6	1.5	1.5	69.1	70.6		
								7	0.43	0.43	70.6	71.03		
								CC	0.25	0.25	71.03	71.28	PAL	
									9.68	9.68				
10X	2	1820	71.2	80.9	9.7	6.18	63.7							
								1	1.5	1.5	71.2	72.7		
								2	1.5	1.5	72.7	74.2	IW	
								3	1.29	1.29	74.2	75.49	HS	
								4	1	0.83	75.49	76.32		

Table T1 (continued).

Core	Date (September 1998)	Time (UTC)	Core depth (mbsf) Top	Core depth (mbsf) Bottom	Length (m) Cored	Length (m) Recovered	Recovery (%)	Section	Length (m) Liner	Length (m) Curated	Section depth (mbsf) Top	Section depth (mbsf) Bottom	Catwalk samples	Comment
								5	0.66	0.66	76.32	76.98		
								CC	0.23	0.23	76.98	77.21	PAL	
									6.18	6.01				
11X	2	1940	80.9	90.5	9.6	6.32	65.8							
								1	1.5	1.5	80.9	82.4		
								2	1.5	1.5	82.4	83.9	IW	
								3	1.5	1.5	83.9	85.4	HS	
								4	1.5	1.5	85.4	86.9		
								5	0.22	0.22	86.9	87.12		
								CC	0.1	0.1	87.12	87.22	PAL	All to PAL
									6.32	6.32				
12X	2	2245	90.5	100.1	9.6	3.81	39.7							
								1	1.5	1.5	90.5	92	IW	
								2	1.5	1.5	92	93.5	HS	
								3	0.71	0.71	93.5	94.21		
								CC	0.1	0.1	94.21	94.31	PAL	Other
									3.81	3.81				
13X	3	100	100.1	109.7	9.6	0.39	4.1							
								CC	0.39	0.39	100.1	100.49	PAL	
									0.39	0.39				
14X	3	330	109.7	119.4	9.7	0.56	5.8							
								CC	0.56	0.56	109.7	110.26	PAL	
									0.56	0.56				
15X	3	545	119.4	126	6.6	2.93	44.4							
								1	1.5	1.5	119.4	120.9	IW	
								2	1.14	1.14	120.9	122.04	HS	
								CC	0.29	0.29	122.04	122.33	PAL	
									2.93	2.93				
16X	3	800	126	130	4	1.3	32.5							
								1	1.2	1.2	126	127.2	HS	
								CC	0.1	0.1	127.2	127.3	PAL	All to PAL
									1.3	1.3				
17X	3	1155	130	139.7	9.7	4.47	46.1							
								1	1.5	1.5	130	131.5		
								2	1.5	1.5	131.5	133	IW	
								3	1.17	1.17	133	134.17	HS	
								CC	0.3	0.3	134.17	134.47	PAL	
									4.47	4.47				
				Totals:	139.7	87.86	62.90							

Notes: PAL = paleontology, IW = interstitial water, HS = headspace. This table is also available in **ASCII format.**

Table T2. Identification and abundance of nannofossils observed at Site 1121.

Core, section, interval (cm)	Depth (mbsf)	Preservation	Group abundance	Bicolumnus ovatus	Bomolithus elegans	Calcidiscus leptoporus	Chiasmolithus bidens	Chiasmolithus danicus	Chiasmolithus spp.	Coccolithus pelagicus	Cruciplacolithus tenuis	Cyclicargolithus abisectus	Dictyococcites antarcticus	Dictyococcites bisectus	Dictyococcites productus	Ellipsolithus macellus	Fasciculithus billii	Fasciculithus bobii	Fasciculithus janii	Fasciculithus tympaniformis	Fasciculithus ulii	Fasciculithus spp.	Gephyrocapsa parallela	Gephyrocapsa (small)	Heliolithus cantabriae	Heliolithus kleinpellii	Heliolithus redelii	Hornibrookina australis	Markalius astroporus	Neochiastozygus concinnus	Neochiastozygus perfectus	Neochiastozygus spp.	Prinsius bisulcus	Reticulofenestra spp.	Reticulofenestra (small)	Sphenolithus primus	Toweius eminens	Toweius pertusus	Toweius selandianus	Toweius spp.	Transversopontis sigmoidalis	Comments
181-1121A-																																										
1H-1, 0-2	0.02		B																																						Barren
1H-1, 4-6	0.05	G	B			T							T	T		T					T	T													T						< 0.8 Ma
1H-CC, 22-27	8.32	G	R											T		T																										> 1.8 Ma
181-1121B-																																									
1H-CC, 11-22	9.81	G	R							F		C																								C						> 1.8 Ma
2H-CC, 12-17	19.38	P	R							T																																> 1.8 Ma
3H-CC, 10-15	28.78		B																																							> 1.8 Ma
4X-CC, 23-28	23.23		R										T	T																						T						> 1.8 Ma
5X-CC, 22-27	23.72		B																																							> 1.8 Ma
6X-1, 2-2	32.72	M	A	R	R				C	A	F								F	C	C								R	A	C				C				A			NP8
6X-1, 107-107	33.77	M	A	R				F	A	A	C								F									R	D	C				C				A			NP8
6X-1, 135-135	34.05	M	C						C	A	F								F	C	C								R	C	C				C			C	A			NP8
6X-2, 10-10	34.30	M	F					F		A																				R		R								T			NP8
6X-CC, 17-27	37.18	M	R																R											R													NP8
7X-CC, 13-23	50.55	M	C						C										F											C									A			NP7–6
8X-3, 16-16	53.71	M	F													R		R	R																			A	A			NP7–6
8X-CC, 11-21	60.96	M	F				C	C		R						?		R	R	F																D					NP7–6
9X-CC, 15-25	71.18	M	C				C	F	F											R					C				C	F	C		F	C				C	C		NP7–6
10X-CC, 0-10	76.98	M	C				C	F		C			C					C												C	C			C	C				C	R		NP7–6
11X-CC, 0-10	87.12	M	C		R		C	F	F														F	F		C				C	F			C	C	C			C	C		NP5
12X-CC, 5-10	94.26	M	F				C	C	C									F					F						C	D			F	C				C			NP5
13X-CC, 34-39	100.44	M	F				C	C	F																				R	C	A			C	C	C			C			NP5
14X-CC, 51-56	110.21	M	F		R		C	C	F	R								R	R										C	D			F	C	C		C	C	C		NP5
15X-CC, 44-49	122.30	M	A				C	C	C	R						F		R	R										C	D			C	C	C		C	C	C		NP4
16X-CC, 0-10	127.20	M	A				C	C	C							F													C	A			C	C	C		C	C	C		NP4
17X-CC, 25-30	134.42	M	F				C	C	R									R	R	R									C	A			C	C				C	C		NP4

Note: Preservation: G = good, M = moderate, and P = poor; total (group) and relative abundance of calcareous nannofossils: D = dominant, A = abundant, C = common, F = few, R = rare, T= trace, and B = barren.

Table T3. Identification and abundance of Paleocene foraminifers observed at Site 1121.

Core, section, interval (cm)	Depth (mbsf)	Alabamina creta	Allomorphina conica	Anomalinoides piripaua	Arenobulimina dorbignyi	Bolivinopsis spectabilis	Charltonina acutimarginata	Conotrochammina whangaia	Cribrostomoides trinitatensis	Dorothia oxycona	Dorothia sp.	Gavelinella beccariiformis	Glomospira charoides	Hormosina ovulum	Lenticulina spp.	Nuttallides carinotruempyi	Nuttallides florialis	Oolina spp.	Oridorsalis umbonatus	Pullenia bulloides	Reticulophragmium paupera	Rzehakina epigona	Valvulineria teuriensis
181-1121B-																							
?11X-CC, 0-10	87.12											R				R						R	
12X-CC, 5-10	94.26				R																		
13X-CC, 34-39	100.44	R					R					R			T			T	R			T	F
14X-CC, 51-56	110.21						T					R											
15X-CC, 44-49	122.28	R	T				T	R		T		C	T	T	R	R			R	R	T	R	F
16X-CC, 0-10	127.20			T		T		T		T		C	T		R	C	F	T	R		T	T	
17X-CC, 25-30	134.42			T	T	T			T		T	T	T		T							T	

Note: C = common, F = few/frequent, R = rare, T = trace, and B = barren.

Table T4. Identification and abundance of diatoms observed at Site 1121.

Core, section, interval (cm)	Depth (mbsf)	Abundance of zeolites	Group abundance	Actinocyclus ingens	Actinocyclus karstenii	Arachnoidiscus sp.	Aulacodiscus sp.	Azpeitia endoi	Coscinodiscus bulliens	Coscinodiscus uralensis	Craspedodiscus sp.	Denticulopsis dimorpha	Denticulopsis hustedtii	Denticulopsis sp.	Diploneis sp.	Eucampia antarctica	Fenestrella sp.	Goniothecium sp.	Hemiaulus incurvus	Hemiaulus kristofferseni	Hemiaulus rossicus	Hemiaulus sp. 2 Fenner (1991)	Hemiaulus velatus	Hemiaulus? beatus	Hemidiscus karstenii	Hemidiscus karstenii f. 1	Hemidiscus ovalis	Hyalodiscus sp.	Nitzschia barronii	Nitzschia denticuloides	Nitzschia interfrigidaria	Nitzschia kerguelenis	Nitzschia praeinterfrigidaria	Nitzschia reinholdii	Nitzschia weaveri	Odontotropis sp.	Pterotheca aculeifera	Rhizosolenia cretacea	Rhizosolenia hebetata f. hiemalis	Rhizosolenia longispina	Rocella vigilans	Simonseniella barboi	Stellarima primalabiata	Stephanopyxis grossecellulata	Stephanopyxis hyalinomarginata	Stephanopyxis turris turris	Thalassiosira complicata	Thalassiosira elliptipora	Thalassiosira fasciculata	Thalassiosira insigna	Thalassiosira inura	Thalassiosira kolbei	Thalassiosira lentiginosa	Thalassiosira oestrupii	Thalassiosira oliverana	Thalassiosira vulnifica	Thalassiosira webbii	Triceratium mirabile	Trinacria aries	Trinacria senta	Trinacria simulacrum
181-1121B-																																																														
?1H-1, 0-2	0.01	B	C																						T															T				T																		
1H-1, 20-20	0.20	B	C	T			R									F										R					C									T				T										C							
1H-1, 54-54	0.54	B	C		C											F	R								F				F	C																		C	R				C	F		F	F			
1H-1, 89-90	0.90	B	C		C											R	R								F				R	C	C										R								R				F			F	F			
1H-1, 100-102	1.00	B	C	C	R								T			R	R								F	R		T	F		F											R						F	F					R	F	R		F	
1H-1, 120-122	1.20	B	C	C	R	T							T	R										F				F					R	R							R					F	F										
1H-1, 140-142	1.40	B	C	F									T	T	T	R								R	F			F				R	R	T							R			T	R		F	F	R	F		R						
1H-2, 20-22	1.70	B	C	F										T	R									R		F			R					R	F						T	R		T	R		R	F						R				
1H-2, 40-42	1.90	B	C											T	T									R		R	R		F			R		F							T				R		R	R									
1H-2, 60-62	2.10	B	C					R						F	F	R								R				F			R		R	T	T						R						R										
1H-2, 80-82	2.30	B	C											F	R													F					R	T	T						F																
1H-2, 100-102	2.50	B	C		R		R							R										R				F				R	F	F						F						R					R						
1H-2, 120-122	2.70	B	F				R	R						R	R									R				F					F	F						R					R	R				T						
1H-2, 140-142	2.90	B	F	R			R							R														F		T	T	F								R						R				R	T				R			
1H-7, 72-72	9.52	D	B																																																										
1H-CC, 6-8	9.76	C	T																																																										
1H-CC, 11-22	9.81	D	B																																																			T								
2H-CC, 12-17	19.38	D	B																																																										
3H-CC, 10-15	28.78	D	B																																																										
4X-CC, 23-28	23.23	F	B																																																										
6X-1, 0-2	32.70	B	F							T									F	T			T	R	T																		S							T		F								F		F
6X-2, 60-65	34.80	B	C		T				R										R					R								R	R	T											R		R		R									R	F
6X-3, 80-	36.50	B	C																F	T			R	R	T																	T			R	R	C	F									C	R	R
6X-CC, 17-27	37.18	B	D		R				R	R	T							R	T			C	F	T	F	F	F								R	R									R	R	F	R	R	T	R					T		F	F
7X-CC, 13-23	50.55	B	F																C	T			F	R																										R	R							R	F
8X-CC, 11-21	60.96	B	D		R	T			C		R								F	R			T																							R	R	R								F	F
9X-CC, 15-25	71.18	B	B		T	T			F		R				R				F	R														R												R	F	R								F	F
10X-CC, 0-10	76.98	B	C		R				F		R								F															R	T											F	F									F	F
11X-CC, 0-10	87.12	B	C						R		R								T															R	T											F										F	F
12X-CC, 5-10	94.26	D	B																																																										
13X-CC, 34-39	100.44	R + chert	B																																																										
14X-CC, 51-56	110.21	R + chert	B																																																										
15X-CC, 24-29	122.28	B	B																																																										
16X-CC, 0-10	127.20	B	B																																																										
17X-CC, 25-30	134.42	B	T																																																										

Note: Zeolite and diatom abundance: D = dominant, A = abundant, C = common, F = few, R = rare, T = trace, and B = barren.

Table T5. Identification and abundance of radiolarians observed at Site 1121.

Core, section, interval (cm)	Depth (mbsf)	Radiolarian zone	Preservation	Group abundance	Amphipyndax stocki	Amphisphaera coronata s.l.	Amphisphaera goruna	Amphisphaera kina	Amphisphaera sp.	Antarctissa denticulata	Antarctissa strelkovi	Axoprunum angelinum	Axoprunum sp.	Bathropyramis sanjoaquinensis s.l.	Buryella foremanae	Buryella granulata	Buryella sp.	Buryella cf. tetradica (3 segments)	Buryella tetradica (4 segments)	Clathrocyclas australis	Cornutella californica	Corythomelissa adunca	Cycladophora pliocenica	Cyrtocapsa campi	Dictyomitra andersoni	Dictyomitra multicostata	Dictyophimus sp.	Dorcadospyris aff. confluens	Euchitonia sp.	Eucyrtidium calvertense	Lithelius nautiloides	Lithomelissa? aitai	Lithomespilus coronatus	Microsciadiacapsa sp.	Myllocercion acineton	Phorticium clevei	Prunopyle antarctica	Pterocodon sp.	Rhopalocanium aff. ornatum	Siphocampe altamontensis	Sphaeropyle sp.	Spongodiscus osculosus	Spongodiscus sp.	Spongoplegma antarcticum	Spongotrochus glacialis	Triceraspyris antarctica
181-1121A-																																														
1H-1, 0-2			VG	A						R	R	T								A										R	C	R					T	R				R	F	C	A	C	R
1H-CC, 22-27	8.32			B																																										
181-1121B-																																														
1H-CC, 1-3	9.71		G	T	R																																								
1H-CC, 6-8	9.76			B																																										
1H-CC, 11-22	9.81		P	T																																										
2H-CC, 12-17	19.38		P	R	R			R																												T										
3H-CC, 10-15	28.78		P	R			R														R	R	R												F						R						
4X-CC, 23-28	23.23		G	T	T				T																																					
5X-CC, 22-27	23.72			B																																										
6X-2, 60-65	34.8	RP6	VG	A	R	A	F			A					T	R		F	C	R	F	F								F	R				C				R					A		
6X-CC, 17-27	37.18	RP6	VG	A	R	A	C	F		F						C		R	C	T	F	F			R	R				C	F				C	C			R					A		
7X-CC, 13-23	50.55	RP6	M	A	R	A				F						C		A	C	T													R		R	A			C					A		
8X-CC, 11-21	60.96	RP6	M	A	C	A	R			C						R		C	C	R	T														C	R			F					C		
9X-CC, 15-25	71.18	RP6	G	A	R	R	F			A	R							R	R	R	F												R	C			F					A		
10X-CC, 0-10	76.98	RP6	VG	A	R	C	C			C	F				R	R		A	A	F	R								R	R				C				R	F			A		
11X-CC, 0-10	87.12	RP6	VG	A	A			C		F								F	C	C	R	R												C	F	A		R				A		
12X-CC, 5-10	94.26		M	R	R			R																											C								R		
13X-CC, 34-39	100.44		M	R	R			R																																					
14X-CC, 51-56	110.21		P	T		R																																							
15X-CC, 24-29	122.28	RP5	M	C	R	C	R								R	R		R																				R				C		
16X-CC, 0-10	127.2	RP4	P	C	R	F	C								R	R	T								R																	C		
17X-CC, 25-30	134.42	RP4	P	F		C	F								F	R									R																	C		

Note: Preservation: VG = very good, G = good, M = moderate, and P = poor; abundance of radiolarians: A = abundant, C = common, F = few, R = rare, T = trace, and B = barren.

Table T6. Composition of interstitial waters, Site 1121.

Core, section, interval (cm)	Depth (mbsf)	Salinity	Cl⁻ (mM)	pH	Alkalinity (mM)	Na⁺ (mM)	Mg²⁺ (mM)	Ca²⁺ (mM)	SO₄²⁻ (mM)	HPO₄²⁻ (μM)	NH₄⁺ (μM)	H₄SiO₄ (μM)	K⁺ (mM)	Li⁺ (μM)	Sr²⁺ (μM)
181-1121B-															
1H-4, 145-150	5.95	34.5	554	7.64	2.83	471	52.0	10.6	28.0	1.5	23	588	13.2	27	92
2H-4, 140-150	15.40	34.5	565	7.58	2.90	478	53.3	11.9	28.2	1.1	50	597	12.6	27	105
3H-4, 140-150	24.90	34.5	562			471	54.2	12.3	27.8	1.1	47	623	13.2	27	110
6X-1, 140-150	34.10	34.5	562	7.56	3.22	470	54.1	12.9	26.9	0.9	24	661	11.0	28	114
7X-3, 140-150	46.70	34.5	562	7.56	2.70	478	51.1	12.3	26.9	0.9	17	676	11.1	28	113
8X-4, 140-150	57.90	34.5	563	7.58	2.77	476	51.4	13.4	26.8	0.9	53	738	10.5	29	124
9X-4, 140-150	67.50	34.5	562	7.60	2.76	477	51.1	12.9	26.7	0.7	17	716	10.1	29	126
10X-2, 140-150	74.10	34.5	562	7.70	3.37	475	51.3	13.8	26.7	0.7	23	700	9.8	29	125
11X-2, 140-150	83.80	34.5	564	7.49	2.97	474	51.4	14.6	26.0	0.9	83	757	10.0	32	141
12X-1, 140-150	91.90	34.5	561	7.55	3.20	475	50.1	13.9	26.0	1.1	86	674	9.7	32	139
15X-1, 140-150	120.80	34.0	557	7.60	3.29	464	49.1	16.9	24.2	1.1	187	599	8.3	45	174
17X-2, 140-150	132.90	34.5	549	7.60	3.17	458	47.3	16.6	23.0	2.1	96	742	8.1	48	176

Note: This table is also available in **ASCII format.**

Table T7. Inorganic carbon, carbonate, total carbon, total organic carbon, total nitrogen, total sulfur, and atomic organic carbon/ nitrogen values for sediments from Holes 1121A and 1121B.

Core, section, interval (cm)	Depth (mbsf)	IC (%)	CaCO$_3$ (%)	TC (%)	TOC (%)	TN (%)	TS (%)	[C/N]$_a$ (%)
181-1121A-								
1H-3, 25-26	3.25	0.07	0.55					
1H-5, 89-90	6.89	0.05	0.38	0.41	0.36	0.03	ND	16.3
1H-6, 6-7	7.56	0.07	0.58					
181-1121B-								
1H-3, 92-93	3.92	0.06	0.52					
1H-5, 48-49	6.48	0.09	0.75					
1H-5, 68-69	6.68	0.08	0.68					
1H-CC, 2-3	9.72	0.08	0.63					
1H-CC, 8-9	9.78	0.09	0.74					
6X-2, 20-21	34.4	6.25	52.02					
6X-2, 120-121	35.4	4.69	39.04	4.77	0.08	0.02	0.08	4.8
6X-3, 65-66	36.35	0.07	0.59					
7X-4, 70-71	47.5	4.34	36.15					
7X-5, 10-11	48.4	4.58	38.13					
7X-5, 110-111	49.4	5.65	47.03	5.72	0.07	0.02	ND	4.3
8X-1, 70-71	52.7	5.37	44.76					
8X-3, 70-71	55.7	4.25	35.38	4.51	0.26	0.03	ND	10.3
8X-5, 70-71	58.7	0.97	8.07					
9X-1, 70-71	62.3	4.38	36.5					
9X-3, 70-71	65.3	4.47	37.2	4.47	ND	0.02	0.15	NA
9X-5, 70-71	68.3	4.64	38.64					
10X-3, 22-23	74.42	0.37	3.04					
10X-5, 61-62	76.93	2.48	20.68					
11X-1, 101-102	81.91	3.21	26.72					
11X-4, 22-23	85.62	4.24	35.29					
11X-4, 77-78	86.17	4.29	35.76	4.41	0.12	0.03	ND	4.6
15X-2, 13-14	121.03	3.19	26.55					
15X-2, 35-36	121.25	5.14	42.78					
15X-2, 100-101	121.9	4.79	39.88					
16X-1, 28-29	126.28	3.83	31.87	3.95	0.12	0.03	ND	4.7
17X-1, 73-74	130.73	3.4	28.28					
17X-2, 19-20	131.69	3.54	29.53					
17X-2, 137-138	132.87	1.88	15.69					
17X-3, 14-15	133.14	0.12	1.01	0.44	0.32	0.03	ND	12.5

Notes: Carbonate is calculated assuming that all inorganic carbon is calcite. ND = not detected. NA = not available. This table is also available in **ASCII format.**

Table T8. List of index properties measured from Hole 1121B.

Leg	Hole	Core	Section	Interval (cm)	Depth (mbsf)	Wet-water content (%)	Dry-water content (%)	Wet-bulk density (g/cm^3)	Dry density (g/cm^3)	Grain density (g/cm^3)	Porosity (%)	Void ratio
181	1121B	1H	1	116-118	1.16	50.4	101.8	1.479	0.733	2.702	72.9	2.687
181	1121B	1H	4	129-131	5.79	50.8	103.3	1.472	0.724	2.686	73.0	2.708
181	1121B	1H	6	136-138	8.86	49.3	97.3	1.488	0.754	2.660	71.7	2.528
181	1121B	2H	1	122-124	10.72	52.8	112.0	1.444	0.681	2.671	74.5	2.921
181	1121B	2H	3	110-112	13.60	46.1	85.7	1.528	0.823	2.643	68.9	2.211
181	1121B	2H	5	113-115	16.63	56.7	131.1	1.392	0.602	2.634	77.1	3.373
181	1121B	3H	1	143-145	20.43	62.6	167.2	1.322	0.495	2.571	80.8	4.199
181	1121B	6X	1	136-138	34.06	65.6	191.0	1.291	0.444	2.570	82.7	4.793
181	1121B	6X	3	111-113	36.81	73.1	271.1	1.210	0.326	2.389	86.3	6.325
181	1121B	7X	1	133-135	43.63	73.9	283.8	1.208	0.315	2.472	87.3	6.851
181	1121B	7X	4	126-128	48.06	65.5	189.6	1.290	0.445	2.539	82.5	4.700
181	1121B	7X	6	56-58	50.36	64.0	178.1	1.308	0.471	2.589	81.8	4.502
181	1121B	8X	1	142-144	53.42	63.9	176.7	1.311	0.474	2.599	81.8	4.484
181	1121B	8X	3	140-142	56.40	69.3	225.6	1.247	0.383	2.457	84.4	5.414
181	1121B	8X	5	130-132	59.30	67.4	206.9	1.260	0.411	2.413	83.0	4.874
181	1121B	9X	1	139-141	62.99	67.2	204.5	1.268	0.417	2.478	83.2	4.949
181	1121B	9X	3	139-141	65.99	66.7	200.1	1.271	0.423	2.453	82.7	4.793
181	1121B	9X	5	142-144	69.02	65.7	191.6	1.286	0.441	2.528	82.5	4.730
181	1121B	9X	7	30-32	70.90	67.1	204.0	1.267	0.417	2.451	83.0	4.882
181	1121B	10X	1	131-133	72.51	70.7	241.7	1.233	0.361	2.429	85.2	5.735
181	1121B	10X	3	117-119	75.37	70.0	233.8	1.233	0.370	2.362	84.4	5.391
181	1121B	10X	5	54-56	76.86	71.4	250.1	1.236	0.353	2.560	86.2	6.251
181	1121B	11X	1	130-132	82.20	68.4	216.3	1.254	0.396	2.441	83.8	5.156
181	1121B	11X	3	20-22	84.10	67.1	203.9	1.268	0.417	2.461	83.1	4.902
181	1121B	11X	5	15-17	87.05	64.1	178.2	1.295	0.466	2.456	81.0	4.274
181	1121B	12X	1	110-112	91.60	66.2	195.9	1.271	0.430	2.414	82.2	4.618
181	1121B	12X	3	23-25	93.73	58.7	142.4	1.374	0.567	2.677	78.8	3.722
181	1121B	15X	1	23-25	119.63	40.9	69.2	1.592	0.941	2.584	63.6	1.747
181	1121B	15X	2	8-10	120.98	39.6	65.5	1.600	0.967	2.534	61.8	1.620
181	1121B	16X	1	24-26	126.24	40.3	67.4	1.606	0.959	2.602	63.1	1.713
181	1121B	17X	1	131-133	131.31	37.6	60.3	1.716	1.070	2.895	63.0	1.705
181	1121B	17X	3	99-101	133.99	40.6	68.3	1.472	0.875	2.100	58.3	1.400

Note: This table is also available in **ASCII format.**